

# Mineralogical and elemental geochemical characteristics of Taodonggou Group mudstone in Taibei Sag, Turpan-Hami Basin: Implication for its formation mechanism

Huan Miao<sup>1,2\*</sup>, Jianying Guo<sup>3\*</sup>, Yanbin Wang<sup>4</sup>, Zhenxue Jiang<sup>1,2</sup>, Chengju Zhang<sup>1,2</sup>, Chuanming Li<sup>1,5</sup>

<sup>1</sup>State Key Laboratory of oil and gas resources and exploration, Beijing 102249, China;

<sup>2</sup>Institute of unconventional oil and gas science and technology, China University of Petroleum (Beijing), Beijing 102249, China;

<sup>3</sup> CNPC Key Laboratory of Natural Gas Accumulation and Development, Langfang 065007, China;

<sup>4</sup>School of Geosciences and Surveying Engineering, China University of Mining and Technology (Beijing), Beijing 100083, China;

<sup>5</sup>College of Geosciences, China University of Petroleum (Beijing), Beijing 102249, China;

*Correspondence to:* Huan Miao(1627765379@qq.com); Jianying Guo ([gyj\\_17711224@petrochina.com.cn](mailto:gyj_17711224@petrochina.com.cn))

**Abstract.** Organic matter types in the Taodonggou Group mudstone exhibit significant differences with depth. In order to understand the formation mechanism of this special phenomenon, we analyzed the mineralogy and geochemistry of the mudstone, as well as the source rocks, depositional environment, and depositional processes of the Taodonggou Group. Based on this, we have gained the following understanding: (1) The Taodonggou Group mudstone was deposited in an intermediate-depth or deep, dyoxic, freshwater-brackish lake environment under warm and humid paleoclimatic conditions. The input of terrestrial debris was stable, but the sedimentation rate was slow. In addition, the sedimentation in the middle stage was influenced by hydrothermal activities, and the changes in the depositional environment corresponded to variations in organic matter types. (2) The source rocks of the Taodonggou Group mudstone are mainly andesitic and feldspathic volcanic rocks. Sediment sorting and recycling were weak, and hydrocarbon source information was well preserved. The tectonic background of the source area was a continental island arc and an oceanic island arc. Furthermore, changes in the provenance of the Taodonggou Group also had a significant impact on the variations in organic matter types. (3) The sedimentation of the Taodonggou Group involved both traction and gravity flows. The variations in source area, depositional environment, and depositional processes during different depositional periods led to changes in the organic matter types of the Taodonggou mudstone. (4) Based on the depositional environment, provenance, and depositional processes, the sedimentation of the Taodonggou Group can be divided into three stages. In the early stages, the sedimentation center was in the Bogda area. At this time, the Bogda Mountain region was not exposed, and the depositional processes inherited the characteristics of Early Permian gravity flow sedimentation, resulting in the widespread deposition of a series of high-quality Type III source rocks in the basin. In the middle stage of the Taodonggou Group sedimentation, the sedimentation center gradually migrated to the Taibei Sag. During this period, the Bogda Mountain region experienced uplift and hydrothermal activity, and the depositional processes gradually transitioned to traction flows, resulting in the widespread deposition of a series of Type II source rocks in the basin. In the late stage of the Taodonggou Group, the uplift of the Bogda Mountain region ceased, and the sedimentation

center completely shifted to the Taibei Sag. Meanwhile, under the influence of gravity flows, the organic matter types of the Taodonggou mudstone changed to Type III.

**Keyword:** Turpan-Hami Basin; Taodonggou Group; Mineralogy; Element Geochemistry; Sedimentary Environment; Source sink system

## 1 Introduction

Turpan-Hami Basin, Junggar Basin and Bogda area all belong to the southern part of the ancient Asian ocean in the Paleozoic era (Korobkin and Buslov, 2011; Jiang et al., 2015). During the Early Carboniferous to Early Permian, they began momentarily to separate due to the continuous expansion of the Bogda Rift and began to enter the basin-forming period in the Middle Permian (Miao et al., 2004; Novikov, 2013; Jiang et al., 2015; Wang et al., 2019; Zhang et al., 2019). The Middle Permian is a momentous stage in the tectonic evolution of the Turpan-Hami basin. During this period, the expansion of the Bogda Rift stopped. With the gradual withdrawal of seawater from Xinjiang, the sedimentary environment of the Turpan-Hami basin gradually shifted to continental facies, and the sedimentary center gradually shifted from the Bogda area to Taibei Sag (Miao et al., 2004; Shi et al., 2020; Li et al., 2022). Taodonggou Group mudstones are widely deposited in the Turpan-Hami Basin. Previous studies have confirmed that Taodonggou Group mudstone is a very good to excellent source rock with huge hydrocarbon generation potential (Song et al., 2018; Miao et al., 2021; Miao et al., 2022; Miao et al., 2022a). It has been found that the organic matter types of the Taodonggou mudstone can be classified into two categories, with the upper and lower sections being Type III and the middle section being Type II (Miao et al., 2021; 2023).

The hydrocarbon generation potential of mudstone is closely related to its sedimentary environment (Wu et al., 2021; Li et al., 2022; Zhang et al., 2019; Zhao et al., 2021; Miao et al., 2004). Regarding the sedimentary environment of the Taodonggou Group mudstone, previous researchers have conducted extensive research. Miao et al. (2004) believed that the mudstone in the Taodonggou Group was deposited in a warm and humid paleoclimate, high-salinity water bodies, and an anoxic environment. Yang et al. (2010), based on the sedimentary characteristics of the Taerlang Formation and the Daheyan Formation, believed that the Taodonggou Group was deposited in a subhumid climate and that climate change is periodic. Wei (2015) also confirmed that the paleoclimate change of the Taodonggou Group stratum has a cyclical feature through tree rings and is mainly a warm and humid paleoclimate. At the same time, Song et al. (2018) also confirmed this by using the elemental geochemical characteristics of the Taodonggou Group shale outcrops in the field; Tian et al. (2017) analyzed the biomarkers of the Taodonggou Group in 7 outcrops around the Turpan-Hami Basin and concluded that the mudstone of the Taodonggou Group was deposited in a balanced, filled lake with little or no terrestrial organic matter, a large amount of algal organic matter input, and weakly alkaline, hypoxic to hypoxic brackish water. Miao et al. (2021) found biomarkers in the Taodonggou Formation mudstone from wells YT1 and L30 from different perspectives of Tian, which may be related to the

63 weathering effect of outcrop samples. Through the research of the above scholars, we have found that there is some  
64 controversy over the sedimentary environment of the Taodonggou Group, and the relationship between the cyclic changes in  
65 the sedimentary environment and the changes in the organic matter types of the Taodonggou Group mudstone is still unclear.

66 In addition, the provenance and sedimentation mode of sediments also have a significant influence on the organic matter  
67 types in mudstones (Mei et al., 2020). Mudstone belongs to a category of fine-grained sediment that is challenging to analyze  
68 using traditional heavy mineral analysis methods (Rollinson, 1993; Roser and Korsch, 1988; Gehrels et al., 2008). Therefore,  
69 elemental geochemical methods can be employed for provenance analysis (McLennan et al., 1983; Kröner et al., 1985; Li et  
70 al., 2020). Elemental geochemical analysis compares the major, trace, and rare earth element characteristics of mudstones in  
71 the sedimentary area with those of lithologies in the provenance area to determine the lithology of source rocks, weathering  
72 degree, and tectonic background of the sediment source area (Li et al., 2020; Floyd and Leveridge, 1987; Basu et al., 2016).  
73 Previous studies have found that the sediment source not only affects variations in the salinity of lake water but also influences  
74 the input of nutrients and terrestrial organic matter, thus impacting the quality of mudstones (Li et al., 2020; Deditius, 2015;  
75 Essefi, 2021). The tectonic activity in the source area not only affects changes in the sedimentary center but also influences  
76 the source area (Miao et al., 2022b; Pinto et al., 2010). Therefore, reconstructing the location and sedimentation mode of the  
77 sediment source area is of great significance for understanding the variations in organic matter types in the Taodonggou Group  
78 mudstones.

79 Based on the mineralogical and elemental geochemical characteristics of 16 mudstone samples collected from the YT1  
80 well, this study aims to reconstruct the paleoclimatic features, provenance, and tectonic background of the sedimentary period  
81 in the source area of the Taodonggou Group mudstones. It also aims to explore the influence of sedimentary environment,  
82 provenance changes, and sedimentation mode on the deposition of the Taodonggou Group mudstones, in order to reveal the  
83 formation process of the mudstones.

## 84 **2 Geological setting**

85 The Turpan-Hami Basin, located in the eastern part of Xinjiang Uygur Autonomous Region, is one of the three major  
86 petroliferous basins in Xinjiang. It is 660 km long from east to west and 130 km wide from north to south, with a total covered  
87 area of  $5.35 \times 10^4$  km<sup>2</sup>. The Turpan-Hami Basin has undergone four stages: the extensional rift basin development stage, the  
88 compressional foreland basin development stage, the extensional faulted basin development stage, and the compressional  
89 regenerated foreland basin development stage, which finally formed the current pattern of the Mesozoic-Cenozoic  
90 superimposed composite inland basin (Zhu et al., 2009; Jiang et al., 2015; Wartes et al., 2002; Greene et al., 2005). According  
91 to the tectonic evolution characteristics of the Turpan-Hami Basin, the Turpan-Hami Basin can be divided into three primary  
92 tectonic units from east to west: the Hami Depression, the Liaodun Uplift, and the Turpan Depression (Miao et al., 2021; Fig.  
93 1a).

94 Taibei sag, the secondary sag of Turpan depression in Turpan-Hami basin, is the largest sedimentary unit in Turpan-Hami  
95 basin (Fig. 1b). The Taibei sag is a Paleozoic-Cenozoic inherited subsidence area (Li et al., 2021), which is a key area for oil  
96 and gas exploration in the Turpan-Hami Basin due to its high thermal evolution degree of hydrocarbon source rocks, good  
97 reservoir physical properties, good cap sealing, and rich oil and gas resources, which are the focus of oil and gas exploration  
98 in the Turpan-Hami Basin. (Wu et al., 2021; Li et al., 2021). Taodonggou Group is the general name of the Daheyan Formation  
99 and the Taerlang Formation. The Daheyan Formation is composed of a sequence of sandstone and conglomerate deposits,  
100 with locally interbedded gray to dark gray mudstone. It is unconformably overlain by the Yierxitu Formation. The Taerlang  
101 Formation is predominantly composed of gray-black mudstone, with localized occurrences of gray-green siltstone and  
102 medium-grained sandstone. Due to the fact that the stratigraphic boundary between the Taerlang Formation and the Daheyan  
103 Formation is not obvious, they are collectively called the Taodonggou Group. The Middle Permian Taodonggou Group is  
104 mainly located in the western part of the study area. At present, only the YT1 and L30 wells are drilled (the YT1 well is drilled  
105 through; the L30 well is not drilled through). The burial depth of the stratum is 4000–6500 m, and the thickness of the  
106 mudstone is 50–200 m (Miao et al., 2022b).

### 107 **3 Samples and experiments**

#### 108 **3.1 Samples**

109 In this study, 16 mudstone samples were collected from well YT1, numbered YT1-1 to YT1-16 in order of depth. After  
110 cleaning the samples, XRD, XRF and ICP-MS experiments were conducted.

#### 111 **3.2 Experiments**

112 The XRD experiment was carried out at Hangzhou Yanqu Information Co., Ltd. The experimental instrument was the  
113 Ultima VI XRD testing instrument of Japanese Neo-Confucianism. In accordance with the Chinese industry standard SY/T  
114 5163-2018, the mudstone was broken to a particle size of less than 200 meshes, and 2 g of samples were weighed to obtain  
115 XRD images through Cu/K $\alpha$  radiation at a scanning speed of 2 °/min. The measurement angle range was  $3^\circ \leq 2\theta \leq 70^\circ$ , and  
116 finally, quantitative interpretation is made with the software X'Pert Highscore Plus of Panalytic Company.

117 The XRF experiment was conducted in Hangzhou Yanqu Information Co., Ltd., and the experimental instrument was a  
118 Panalytical Axios tester from Panalytical. The mudstone was first crushed to a particle size of less than 200 meshes, then 10  
119 g of the sample was weighed and calcined in a muffle furnace for 4 hours to get rid of organic matter and carbonates, weighed  
120 and recorded the weight loss, and finally Li<sub>2</sub>B<sub>4</sub>O<sub>7</sub> was added, mixed evenly and made into glass bead, and the main element  
121 concentration was tested.

122 The ICP-MS test was performed at Beijing Orient Smart, and the test instrument was an ELEMENT XR inductively  
123 coupled plasma emission spectrometer manufactured by Thermo Fisher, Inc. Before analysis, the samples were ground to a  
124 particle size of less than 40  $\mu$ m. An appropriate amount of the sample was weighed and dissolved in HF (30%) and HNO<sub>3</sub>  
125 (68%) at 190°C for 24 hours. After evaporating the excess solvent with deionized water, the solution was redissolved in 2 ml

of 6.5% HNO<sub>3</sub>. Redissolve in 2 ml of 6 mol/L HNO<sub>3</sub> and then store at 150 °C for 48 hours. Subsequently, after evaporating the solution, 1 ml of the 6 mol/L HNO<sub>3</sub> evaporated solution was added to the sample.

## 4 Results

### 4.1 Mineralogy

The XRD test results of 16 samples from Well YT1 are shown in Table 1 and Figure 2. As can be seen from Table 1 and Figure 2, Taodonggou Group mudstones are composed of clay, quartz, calcite, plagioclase, barite, and K-feldspar, and some samples contain siderite and pyrite. The content of clay is the highest (23.9%–70.9%, mean 40.78%), followed by quartz (17.2%–59.2%, mean 34.69%), calcite (1%–35.4%, mean 16.97%), barite (0%–13.3%, mean 4.21%), plagioclase (0%–5.4, mean 2.93%), and K-feldspar (0%–2.3, mean 0.9%).

The mineral composition can be used to analyze the lithofacies type of mudstone, and different lithofacies types often have different characteristics (Glaser et al., 2014). Previous scholars believed that mudstone types could be divided by the ternary diagram of mineral composition. The three end elements of the ternary diagram are quartz + feldspar + mica (QFM), calcite + dolomite + ankerite + siderite + magnesite (carbonate), and clay. The XRD results of 16 mudstone samples from Well YT1 in the study area are put into the ternary map (Fig. 3). The results show that the data points of Taodonggou Group mudstone in the study area are located in four areas, namely, mixed mudstone, silica-rich argillaceous mudstone, argillaceous siliceous mudstone and mixed siliceous mudstone, and most of the points are mixed mudstone and argillaceous siliceous mudstone areas, which indicates that Taodonggou Group mudstone can be divided into four types: mixed mudstone, silica-rich argillaceous mudstone, argillaceous siliceous mudstone and mixed siliceous mudstone, and the main lithofacies are mixed mudstone and argillaceous siliceous mudstone.

### 4.2 Major element

Table 2 shows the results of the major elements in 16 mudstone samples from Well YT1. From Table 2, we can see that the major elements of the Taodonggou Group mudstone are mainly SiO<sub>2</sub>, Al<sub>2</sub>O<sub>3</sub>, Fe<sub>2</sub>O<sub>3</sub>, CaO, and TiO<sub>2</sub>. The highest content of SiO<sub>2</sub> is from 43.11% to 70.11%, with an average value of 56.18%. Al<sub>2</sub>O<sub>3</sub> content takes second place, accounting for 11.65% to 25.75%, with an average value of 18.69%; the average content of another main element is less than 10%.

### 4.3 Trace element

The trace element content of the Taodonggou Group mudstone is shown in Table 3. Enrichment factor (EF) is an important indicator of element enrichment (Taylor and McLennan, 1985; Ross and Bustin, 2009). By comparing the trace element content of the mudstone of the Taodonggou Group with the global average shale (AS), the trace element enrichment factors in the study area are calculated as follows:

$$X_{EF} = \frac{(X / Al)_{\text{samples}}}{(X / Al)_{AS}} \quad (1)$$

Where X and Al represent the concentrations of elements X and Al (Taylor and McLennan, 1985; Ross and Bustin, 2009).

157  $X_{EF} < 1$  represents the dilution concentration of element X relative to the standard composition,  $X_{EF} > 1$  represents the relative  
158 enrichment of element X compared to the AS concentration,  $X_{EF} > 3$  represents the detectable autogenetic enrichment, and  
159  $X_{EF} > 10$  is considered an indicator of moderate to strong autogenetic enrichment (Taylor and McLennan, 1985; Ross and  
160 Bustin, 2009).

161 Figure 4 and Table 4 presents the enrichment factors of Taodonggou Group mudstone in the study area. It can be seen  
162 from Figure 4 and Table 4 that only Hf (0.5-2.11, mean = 1.29) is enriched in the Taodonggou Group mudstone compared  
163 with AS, and other elements are no enriched.

#### 164 4.4 Rare earth element

165 The REE content of Taodonggou Group mudstone in the study area is shown in Table 5. According to Table 5, the  $\Sigma$ REE  
166 content of Taodonggou Group mudstone ranged from 43.247 ppm to 257.997 ppm, with an average value of 159.206 ppm.  
167 The light rare earth element (LREE) content was the highest (mean value 133.45 ppm), followed by medium rare earth element  
168 (MREE) (mean value 17.438 ppm) and heavy rare earth element (HREE) (mean value 6.684 ppm) in that order. After chondrite  
169 standardization (Taylor and McLennan, 1985), Taodonggou Group mudstone shows a right dipping REE distribution pattern  
170 (Fig. 5),  $(La/Yb)_N$  is 6.228–10.081, with an average value of 7.358.

171 In addition, in Figure 5, although the YT1-13 sample exhibits a weak right dipping REE distribution pattern similar to  
172 other samples, its rare earth elements are significantly depleted. Based on Figure 4 and Table 4, the trace elements in the YT1-  
173 13 sample are depleted compared to AS, indicating that the YT1-13 sample has been influenced by groundwater leaching.

#### 174 4.5 Reconstruction of paleosedimentary environment based on element geochemical characteristics

##### 175 4.5.1 Paleoclimate and weathering

176 The paleoclimate not only affects the weathering degree of the parent rock but also affects the transport distance of  
177 sedimentary debris and the transport of nutrients (Zhang et al., 2005). There are many evaluation indices for paleoclimate,  
178 such as the chemical alteration index (CIA) and the climate index (C). It is generally believed that when  $CIA=50-65$  and  $C <$   
179  $0.2$ , it reflects that the sedimentary system is in a dry and cold climate under the background of lower of degree of chemical  
180 weathering; when  $CIA=65-85$  and  $0.2 < C < 0.8$ , it indicates that the sedimentary system is in a warm and humid climate  
181 under the background of middle of degree of chemical weathering; when  $CIA=85-100$  and  $C > 0.8$ , it reflects the humid and  
182 hot climate under the background of high of degree of chemical weathering (Zhang et al., 2019; Nesbitt and Young, 1984).

183 The calculation formula for CIA and C is as follows:

$$184 \quad CIA = \frac{Al_2O_3 \times 100}{Al_2O_3 + Na_2O + CaO^* + K_2O} \quad (2)$$

$$185 \quad C = \frac{Fe + Mn + Cr + Ni + V + Co}{Ca + Mg + Sr + Ba + K + Na} \quad (3)$$

186 In formula (2), CaO \* only refers to CaO in silicate minerals. Due to the lack of direct measurement means, it is often  
187 calculated indirectly by the content of  $P_2O_5$ , namely:

$$CaO^* = mol(CaO) - \frac{10}{3} mol(P_2O_5) \quad (4)$$

Where, mol(CaO) and mol(P<sub>2</sub>O<sub>5</sub>) are the mole numbers of CaO and P<sub>2</sub>O<sub>5</sub>, where when mol (Na<sub>2</sub>O) ≤ mol (CaO \*), mol (CaO \*) = mol (Na<sub>2</sub>O); on the contrary, when mol(Na<sub>2</sub>O) > mol(CaO\*), mol(CaO\*)=mol(CaO) (Nesbitt and Young, 1984). The CIA values of the Taodonggou Group mudstone in the study area were calculated based on Equation (2) and Equation (3), ranging from 68.71 to 96.97, with a mean value of 80.17. The climate index (C) is 0.22–2.42 (average = 1.01, Tab.3). The overall paleoclimate was warm, humid, and hot (Fig. 6a).

In addition, the cross plot of Ga/Rb and K<sub>2</sub>O/Al<sub>2</sub>O<sub>3</sub> can also be used to analyze the paleoclimate characteristics during the formation of sedimentary rocks (Lerman and Baccini, 1987; Liu and Zhou, 2007). As shown in the cross plot of Ga/Rb and K<sub>2</sub>O/Al<sub>2</sub>O<sub>3</sub> (Fig. 6b), almost all points are in the warm/wet area, which indicates that Taodonggou Group mudstone was deposited in a warm and humid paleoclimate.

By analyzing the correlations between CIA, C, and Ga/Rb (Figure 6c–e), it can be observed that there is the strongest correlation between CIA and C (Figure 6c, R<sup>2</sup> = 0.7566). Additionally, the correlation coefficients between CIA and Ga/Rb, as well as C and Ga/Rb, are both greater than 0.4 (Figures 6d and 6e). This indicates that CIA, C, and Ga/Rb are reliable indicators of the paleoclimate during the sedimentation of the Taodonggou Group mudstone. Based on the above analysis, the Taodonggou Group mudstone in the study area was deposited in a warm, humid, and hot paleoclimate. This result is consistent with Miao's indicator result using the biomarker parameter CPI (Miao et al., 2021), indicating that the biomarker parameter CPI can be used to explain the paleoclimate change characteristics of hydrocarbon source rocks with Ro ≤ 1.49.

#### 4.5.2 Paleo-redox conditions

Redox environments are critical to the preservation of organic matter in sedimentary rocks, and sensitive elements such as Co, Mo, U, Th, V, Ni, and Cr are commonly used to identify redox conditions in ancient water bodies. Previous evidence suggests that U/Th < 0.75, V/Cr < 2 and V/(V+Ni) < 0.45 represent an oxic conditions, 0.75 < U/Th < 1.25, 2 < V/Cr < 4.25 and 0.45 < V/(V+Ni) < 0.84 represent a dyoxic conditions, U/Th < 1.25, V/Cr < 4.25 or V/(V+Ni) < 0.84 represent an anoxic condition (Hatch and Leventhal, 1992; Rosenthal et al., 1995; Tribovillard et al, 2006; Tribovillard et al, 2012). There is no significant correlation between V, U, and Th and Al<sub>2</sub>O<sub>3</sub> contents in the Taodonggou Group mudstone samples, indicating that V, U, and Th contents in Taodonggou Group mudstone are mainly controlled by authigenic deposition under redox conditions (Tribovillard et al., 1994). The U/Th, V/Cr, and V/(V+Ni) of the Taodonggou Group mudstone range from 0.21 to 0.52 (mean = 0.29), 1.62 to 4.95 (mean = 2.7), and 0.65 to 0.92 (mean = 0.75). In the light of U/Th, Taodonggou Group mudstones were deposited in an oxic environment, and according to V/Cr and V/(V+Ni), Taodong Group mudstones were deposited in a dyoxic environment. This is because U/Th cannot accurately identify the redox environment of the sediments under highly weathered conditions (Cao et al., 2021), so V/Cr and V/(V+Ni) were used in this study to identify the redox environment of Taodonggou Group mudstone. The cross plot of V/Cr and V/(V+Ni) shows (Fig. 7) that Taodonggou Group mudstones were

219 deposited in a dyoxic environment.

#### 220 4.5.3 Paleosalinity

221 Paleosalinity is an important indicator of the paleoenvironment of a water body. The level of paleosalinity affects the  
222 stratification of the sedimentary water body and the development of plankton, thereby affecting the paleoproductivity and  
223 enrichment of organic matter in the sedimentary environment (Thorpe et al., 2012; Wang et al., 2021; Shi et al., 2021).  
224 Previous research has found that Sr/Ba and B/Ga can represent changes in paleosalinity. It is generally believed that Sr/Ba<0.5  
225 or B/Ga<3 represents fresh water, 0.5<Sr/Ba<1 or 3<B/Ga<6 means brackish water, and Sr/Ba>1 or B/Ga>6 represents saline  
226 water. The correlation between Sr and CaO of Taodonggou Group mudstone in the study area is not obvious ( $R^2=0.17$ ), Sr/Ba  
227 of Taodonggou Group mudstone in the study area ranges from 0.32 to 1.83, with an average value of 0.71, and the B/Ga is  
228 2.53–5.81 (average = 3.36), indicating that Taodonggou Group mudstone was deposited in freshwater and brackish water  
229 environments (Fig. 8a).

230 In addition,  $Ca/(Ca+Fe)$  is a reliable indicator for evaluating the salinity of lake waters (Wang et al., 2021). The  
231  $Ca/(Ca+Fe)$  distribution of Taodonggou Group mudstone in the study area ranges from 0.14 to 0.78, with a mean value of  
232 0.42. The Sr/Ba and  $Ca/(Ca+Fe)$  intersection diagram (Fig. 8 b) shows that Taodonggou Group mudstones were deposited in  
233 freshwater and brackish water environments, which is in accord with the Sr/Ba and B/Ga intersection diagram.

#### 234 4.5.4 Paleobathymetry

235 Previous research has shown that some elements of the sedimentation process change dramatically with offshore distance.  
236 These elements can be used to judge the water depth variation during the sedimentation period. The commonly used indicators  
237 are Zr/Al, Rb/K, and MnO content (Xiong and Xiao, 2011; Herkat et al., 2013). It is now believed that the lower the Zr/Al  
238 ratio or the higher the Rb/K ratio, the further offshore and the deeper the water (Xiong and Xiao, 2011; Herkat et al., 2013).  
239 Zr/Al of Taodonggou Group mudstone is  $5.19 \times 10^{-4}$ – $22.51 \times 10^{-4}$  (average =  $13.44 \times 10^{-4}$ ), showing a trend of first decreasing  
240 and then increasing with the depth, Rb/K ranges from  $7.32 \times 10^{-4}$  to  $29.79 \times 10^{-4}$  (mean  $19.02 \times 10^{-4}$ ), with large fluctuations  
241 with depth of burial. The high-value area of Rb/K is basically consistent with the low-value area of Zr/Al, which indicates  
242 that the ancient water depth during the Taodonggou Group mudstone deposition process has a trend of first decreasing and  
243 then increasing.

244 For the content of MnO, it is generally believed that < 0.00094% is a shore lake, 0.00094%–0.0075% is a shallow lake,  
245 0.0075%–0.051% is an intermediate-depth lake, and > 0.051% is a deep lake (Herkat et al., 2013). MnO of Taodonggou Group  
246 mudstone is 0.05%–0.30%, with an average of 0.16 %, which indicates that the Taodonggou Group mudstone are mainly  
247 deposited in intermediate depth - deep lake sedimentary environment.

#### 248 4.5.5 Terrigenous detritus input

249 Ti, Si, and Al are relatively stable during diagenesis and are usually used as indicators of debris flux input (Algeo and



250 Maynard, 2004; Maravelis et al., 2021). Generally, Ti in sediments comes from ilmenite ( $\text{FeTiO}_3$ ) or rutile ( $\text{TiO}_2$ ), while Al  
251 can exist in feldspar, clay minerals, and other aluminum silicate minerals (Algeo and Maynard, 2004). Compared with Ti and  
252 Al, Si comes from many sources, including both biological origin and hydrothermal and terrigenous clastic input (Kidder and  
253 Erwin, 2001). Therefore, when using  $\text{SiO}_2$  as the evaluation index for terrigenous clastic input, its source needs to be analyzed.  
254 The correlation of  $\text{Al}_2\text{O}_3$  and  $\text{TiO}_2$  with  $\text{SiO}_2$  in Well YT1 of the study area is not obvious, which indicates that their sources  
255 are more complex and not dominated by terrestrial debris sources (Fig. 9). Therefore,  $\text{Al}_2\text{O}_3$  and  $\text{TiO}_2$  are used in this study  
256 to indicate the terrestrial debris input during the deposition of the Taodonggou Group mudstone.

257 The  $\text{Al}_2\text{O}_3$  content of YT1 wells is higher, ranging from 11.65 % to 25.75 %, with an average value of 18.69 %; the  $\text{TiO}_2$   
258 is 1.15 %–4.22 % (average = 1.77 %). As can be seen from Table 2, the  $\text{Al}_2\text{O}_3$  content of Well YT1 fluctuates more with depth,  
259 and the overall trend is increasing first and then decreasing with depth, while the  $\text{TiO}_2$  fluctuates less with depth, and on the  
260 whole, the trend is increasing with depth. Combined with the results of paleoclimate analysis in the study area, it is found that  
261 the terrestrial debris input during the deposition of the Taodonggou Group strata has the characteristics of increasing first and  
262 then decreasing.

#### 263 4.5.6 Paleoproductivity

264 Paleoproductivity determines the quantity of original organic matter in sedimentary rocks (Wei et al., 2012; Algeo and  
265 Ingall, 2007; Ross and Bustin, 2009; Schoepfer et al., 2015). The elements P, Si, Ba, Zn, and Cu are indicators of the magnitude  
266 of paleoproductivity, but they all have a certain range of application; for example, only the biogenic parts of Si and Ba can  
267 represent productivity, and Zn can only represent productivity change in the sulfide reduction environment (Wei et al., 2012;  
268 Algeo and Ingall, 2007).

269 P is not only a key nutrient element in biological metabolism but also an important component of many organisms, so it  
270 can also be used to characterize biological productivity (Kidder and Erwin, 2001). P/Ti or P/Al is commonly used to reflect  
271 biological productivity in order to eliminate the influence of terrigenous detritus. The P/Ti of Taodonggou Group mudstone  
272 in the study area ranges from 0.04 to 0.74 percent, with an average value of 0.17 percent and an overall low productivity. As  
273 shown in Table 2, the relationship between P/Ti and depth was analyzed, and the results showed that the paleontological  
274 productivity tended to increase and then decrease with depth.

275 In addition, Cu is also an important nutrient and, unlike P, is generally indicative of productivity, including the sum of  
276 primary productivity and productivity from terrestrial inputs (Schoepfer et al., 2015). For the purpose of eliminating the  
277 dilution interference of terrigenous detritus, Cu/Ti is used as an indicator to evaluate the paleoproductivity in this study. The  
278 distribution range of Cu/Ti of Taodonggou Group mudstone in the study area is from 0.55 to 1.96 with an average value of  
279 1.02 and gradually decreases with depth, indicating a gradual increase in palaeoproductivity during the deposition of  
280 Taodonggou Group mudstone.

#### 281 4.5.7 Deposition rate

282 The deposition rate is one of the parameters characterizing the magnitude of the dilution effect during deposition and is  
283 commonly characterized by  $(La/Yb)_N$ . It is generally believed that the difference between LREE and HREE migration is not  
284 significant when the sedimentation rate of the lake basin is faster and the  $(La/Yb)_N$  value is close to 1. Conversely, when the  
285  $(La/Yb)_N$  value is greater or less than 1, it indicates that the sedimentation rate of the lake basin is slower (Wang et al., 2021;  
286 Cao et al., 2018). The  $(La/Yb)_N$  of the Taodonggou Group mudstones are 6.228–10.081, with an average value of 7.358 in the  
287 study area, which is much greater than 1. This indicates that the mudstone of the Taodonggou Group has a slower deposition  
288 rate.

#### 289 4.5.8 Hydrothermal activity

290 The study area has been extremely volcanically active from the Carboniferous to the Permian, with extensive volcanic  
291 deposits in the Middle Permian Taodonggou Group, the Lower Permian Yierxitu Formation, and the Carboniferous. In order  
292 to explore whether hydrothermal activity is involved in the Middle Permian sedimentation, the Zn-Ni-Co ternary diagram and  
293 the  $(Cu+Co+Ni) \times 10$ -Fe-Mn ternary diagram are applied in this study (Xu et al., 2022; You et al., 2019). Based on the Zn-Ni-  
294 Co ternary diagram (Fig. 10a), some data points of the Taodonggou Group mudstone are distributed in the hydrothermal  
295 sedimentary zone, and based on the  $(Cu+Co+Ni) \times 10$ -Fe-Mn ternary diagram (Fig. 10b), all data points of the samples fall in  
296 the hydrothermal sediment zone and Red Sea hydrothermal sediment zone, which indicates that the Taodonggou Group  
297 mudstone deposition was influenced by hydrothermal fluids.

#### 298 4.5.9 Tectonic setting

299 Sedimentary rocks of different tectonic settings have prominent differences in element composition and content, so the  
300 geochemical characteristics of sedimentary rocks can be used to reflect the tectonic setting of sedimentary basins  
301 (Kroonenberg, 1992).

302 The elements Co, Th, Sc, Zr, and La are relatively stable and less affected by geological activities such as weathering,  
303 transportation, and deposition. Therefore, the La-Th-Sc ternary diagram and the Th-Co-Zr/10 ternary diagram can be utilized  
304 to distinguish the tectonic setting during the formation of sediments (Bhatia and Crook, 1986; Cai et al., 2022). Based on the  
305 La-Th-Sc ternary diagram (Fig. 11a), most of the data points fall in the continental island arc region, and on the Th-Co-Zr/10  
306 ternary diagram (Fig. 11b), almost all the data points fall in the continental island arc and oceanic island arc regions. This  
307 indicates that the tectonic setting of the Taodonggou Group's source area is a continental island arc and an oceanic island arc.

308 Additionally, previous studies have shown that  $SiO_2$ ,  $TiO_2$ ,  $Al_2O_3/SiO_2$  and  $Fe_2O_3+MgO$  are also important parameters  
309 for identifying the source tectonic setting. Cross plots of  $Al_2O_3/SiO_2$  and  $Fe_2O_3+MgO$ ,  $TiO_2$  and  $Fe_2O_3+MgO$ , and  $SiO_2$  and  
310  $Al_2O_3/SiO_2$  are often employed to recognize the tectonic setting (Bhatia, 1983; Li et al., 2020; Roser and Korsch, 1988). Based  
311 on the cross plot of  $Al_2O_3/SiO_2$  and  $Fe_2O_3+MgO$  (Fig. 11c), all data points are distributed around the continental island arc

312 and oceanic island arc, which is consistent with the cross plot of  $\text{TiO}_2$  and  $\text{Fe}_2\text{O}_3+\text{MgO}$  (Fig. 11d) and the cross plot of  $\text{SiO}_2$   
313 and  $\text{Al}_2\text{O}_3/\text{SiO}_2$  (Fig. 11e). As a result, the tectonic setting of Taodonggou Group mudstone source area is continental island  
314 arc and oceanic island arc.

## 315 **5 Discussion**

316 The sedimentary environment, provenance location, and sedimentation mode are factors that influence the quality of  
317 mudstones. In this study, based on the mineralogical and elemental geochemical characteristics of the Taodonggou Group  
318 mudstones, we discuss the influence of sedimentary environment, provenance location, and sedimentation mode on the quality  
319 of the Taodonggou Group mudstones.

### 320 **5.1 The influence of palaeosedimentary environment on the quality of mudstone**

321 Based on the mineralogical, elemental geochemical characteristics and previous studies on the organic geochemical  
322 characteristics of the Taodonggou Group mudstones (Miao et al., 2021), a comprehensive geochemical profile of the YT1  
323 well was established. The results are shown in Figure 12. It can be observed from Figure 12 that the sedimentary environment  
324 of the Taodonggou Group mudstones is closely related to their organic matter types and can be divided into three periods. In  
325 the early stage of the Taodonggou Group, the overall climate was warm and humid under moderate chemical weathering  
326 conditions. The sedimentary water body was dyoxic-anoxic brackish water. At this time, productivity was weak, and organic  
327 matter was mainly derived from terrestrial sources. In the middle stage of the Taodonggou Group, the paleoclimate gradually  
328 shifted to a dry and humid climate under strong chemical weathering conditions, accompanied by hydrothermal activity. This  
329 provided abundant nutrients for the growth of algae and other microorganisms. At the same time, the sedimentation rate  
330 increased, resulting in a predominance of algae in the organic matter composition during this period. During the late stage of  
331 the Taodonggou Group, the climate again shifted to a warm and humid climate under moderate chemical weathering  
332 conditions. The sedimentation rate slowed down, and the input of organic matter shifted back to predominantly terrestrial  
333 sources.

### 334 **5.2 Provenance**

#### 335 **5.2.1 Lithology of parent rock**

336 Previous studies have found that the chemical composition of the rocks in the sedimentary area and the parent rock in  
337 the provenance area have a strong affinity, and the type of parent rock will directly affect the elemental geochemical  
338 characteristics of the sediment (Tribovillard et al., 2006; Shi et al., 2021; McLennan et al., 1993; Basu et al., 2016; Hu et al.,  
339 2021; Floyd and Leveridge, 1987; Wronkiewicz and Condie, 1987). Generally speaking, the transport of sediment from the  
340 source area to the sedimentary area goes through multiple complex processes such as mechanical transport and chemical  
341 action, and hence it is necessary to analyze the impact of sediment sorting and recycling on each chemical component when  
342 identifying the source. Previous studies have shown that trace elements Zr, Th, and Sc are relatively stable in geological

343 processes such as weathering, transportation, and sorting and are not easily lost, which can be used as one of the indicators  
344 for parent rock identification (Floyd and Leveridge, 1987; Wronkiewicz and Condie, 1987). According to the Th/Sc and Zr/Sc  
345 intersection diagram of Taodonggou Group mudstone (Fig. 13a), Taodonggou Group mudstone is close to andesite and felsic  
346 volcanic rock of the upper crust, and its composition is controlled by the composition of its felsic parent rock and has not  
347 undergone sediment sorting and recycling.

348 In addition, REE and trace elements in mudstone from different parent rocks are obviously different, so the ratio of REE  
349 to trace elements can be used to analyze the type of parent rock, and the most common ones are La/Sc, La/Co, Th/Sc, Th/Co,  
350 and Cr/Th (Basu et al., 2016; Hu et al., 2021; Floyd and Leveridge, 1987; Wronkiewicz and Condie, 1987; Allègre and Minster,  
351 1978). Based on the Hf and La/Th intersection diagrams (Fig. 13b) and the La/Sc and Co/Th intersection diagrams (Fig. 13c),  
352 we can see that the mudstones of the Taodonggou Group have both andesitic island-arc sources and felsic volcanic sources.  
353 It can be seen from the cross plot of TiO<sub>2</sub> and Zr (Fig. 13d) that the mudstone of the Taodonggou Group is a source of  
354 intermediate igneous rocks and felsic igneous rocks. As can be seen from the cross plot of La/Yb and  $\Sigma$  REE (Fig. 13e), almost  
355 all data points are located in the sedimentary rock, alkali basalt, and granite areas.

356 In summary, the parent rocks of the Taodonggou Group mudstone are andesitic and feldspathic volcanic rocks with weak  
357 sedimentary sorting and recirculation, and the material source information is well preserved.

#### 358 5.2.2 Location of Parent Rock

359 There is a great deal of controversy about the provenance location of the Middle Permian in Turpan-Hami (Shao et al.,  
360 2001; Jiang et al., 2015; Wang et al., 2019; Zhao et al., 2020; Song et al., 2018; Wang et al., 2018; Tang et al., 2014). Shao et  
361 al. (1999) believed that the provenance of the Permian was mainly from the Jueluotage Mountain in the south of the Turpan-  
362 Hami Basin; Song et al. (2018) considered that it came from the Bogda area; Zhao et al. (2020) believed that the provenance  
363 of the Permian in the Turpan-Hami Basin was consistent with that in Junggar and originated from the Kelameili Mountain  
364 and the Northern Tianshan. Summarizing the previous research results, it is found that the main controversial point is the time  
365 of the first uplift of Bogda Mountain.

366 At present, there are many opinions about the time of the Bogda Mountain uplift. They think that the initial uplift of  
367 Bogda Mountains occurred in Early Permian (Carroll et al., 1990; Shu et al., 2011; Wang et al., 2018; Li et al., 2022), Middle  
368 Permian (Zhang et al., 2006; Liu et al., 2018; Wang et al., 2018), Late Permian-Early Triassic (Zhao et al., 2020; Guo et al.,  
369 2006; Wang, 1996; Sun and Liu, 2009; Tang et al., 2014; Wang et al., 2018), Middle Triassic (Guo et al., 2006), Early Jurassic  
370 (Green et al., 2005; Liu et al., 2017; Ji et al., 2018) and Late Jurassic (Yang et al., 2015). If the initial uplift of the Bogda  
371 Mountains was after the middle Permian, the parent rock types of the Taodonggou Group mudstone in the Turpan-Hami Basin  
372 and the Luchaogou Formation mudstone in the Junggar Basin should be the same.

373 We have counted the element geochemical characteristics of Luchaogou Formation in the Junggar Basin (Li et al., 2020)

374 and found that the parent rock type of Luchaogou Formation mudstone in the Junggar Basin is greatly different from that of  
375 P<sub>2</sub>td, which is felsic volcanic rock (Fig. 14). As a result, Bogda Mountain's initial uplift should be Late Permian-Early Triassic  
376 in the Early Permian or Middle Permian. This is consistent with Li et al. (2022) and Wang et al. (2018), who inferred the uplift  
377 of Bogda Mountain at 289.8 Ma–265.7 Ma. Shao et al. (2001) believed that the sandstone of the Daheyan Formation in  
378 Turpan-Hami Basin has a good affinity with the Early Permian and Carboniferous, so the provenance direction of the  
379 sandstone of the Daheyan Formation is consistent with that of the Early Permian, and they all come from the Jueluotage  
380 Mountain. However, the paleocurrent direction of the Early Permian in Xinjiang is southeast (Zhang et al., 2005; Li et al.,  
381 2007; Wang et al., 2019), and the provenance area is located in the north of the Bogda area. Zhao et al. (2020) calculated the  
382 U-Pb dating results of 5250 zircons in the Tianshan and believed that the provenance of the Turpan-Hami Basin and the  
383 Junggar Basin both came from the northern Tianshan and the Kelameili Mountain, which is also consistent with the ancient  
384 ocean current direction in the Early Permian (Zhang et al., 2005; Li et al., 2007; Wang et al., 2019; Fig. 14a). Consequently,  
385 the first uplift of Bogda Mountain should have occurred in the early Permian, but it was not exposed in the early Middle  
386 Permian, and it still received sedimentation. In the middle Permian, the exposed water began to be denuded, becoming the  
387 source area of the Turpan-Hami Basin (Wang et al., 2018).

388 Based on the above analysis, in the early Middle Permian, although Bogda Mountain in the north of Turpan-Hami Basin  
389 was uplifted due to orogeny, it did not emerge from the water surface, and it still accepted the provenance of North Tianshan  
390 and Kelameili Mountain. At this time, there was a NE-trending ancient ocean current (Carrollet et al., 1995; Obrist-Farnert et  
391 al., 2015; Zhao et al., 2020), so Jueluotage Mountain, which has been uplifted in the south of Turpan-Hami Basin, became a  
392 secondary provenance area (Shao et al., 1999; Fig. 14b). With the continuous uplift of Bogda Mountain, the sedimentary  
393 center of Turpan-Hami Basin gradually shifted to Taibei Sag, and the provenance area of Turpan-Hami Basin changed to  
394 Bogda Mountain and Jueluotage Mountain (Fig. 14c).

### 395 **5.3 sedimentation mode**

396 In previous studies, scholars have believed that the sedimentation of the Permian in the Turpan-Hami Basin is mainly  
397 controlled by traction currents (Chen et al., 2003). However, recent research has revealed the presence of gravity flow deposits  
398 in the Permian of the Turpan-Hami Basin (Wang et al., 2017; Wang et al., 2018; Xu, 2022). Yang et al. (2010) found poorly  
399 sorted debris flow deposits in the Daheyan Formation, and Xu (2022) discovered alluvial and fluvial facies in the Daheyan  
400 Formation, consisting of volcanoclastic rocks and conglomerates that are similar in composition to the Lower Permian  
401 volcanoclastic rocks and conglomerates. This suggests the existence of gravity flow deposits during the early Permian in the  
402 Turpan-Hami Basin. Wang et al. (2018) also suggested the development of gravity flow deposits and pillow lavas in the Early  
403 Permian. Meanwhile, in the early Middle Permian, the sedimentation inherited the provenance and sedimentation style from  
404 the early Permian, but the gravity flow deposits transitioned gradually into traction current deposits. Due to the influence of

405 gravity flow deposits, terrestrial organic matter can be transported to the deep lake area (Yu et al., 2022; Li et al., 2011),  
406 thereby altering the type of organic matter.

407 During the middle of the Taodonggou Group, the Turpan-Hami Basin entered the foreland basin sedimentation stage due  
408 to the uplift of the Bogda Mountains. The sedimentary environment of the Taodonggou Group in the Tainan Sag is similar to  
409 that in the Taibei Sag (Li, 2019). During this time, the sedimentary water body of the Taodonggou Group in the Turpan-Hami  
410 Basin became shallower, and the dominant sedimentation style transitioned to traction currents. Xu (2022) conducted  
411 lithological observations on the Taerlanggou section, the Zhaobishan section, and the Y well in the Taodonggou Group and  
412 found the presence of traction structures of gravity flow origin in the middle and upper parts of the Taerlang Formation.  
413 Additionally, a large number of calcareous and iron nodules appeared in the formation, indicating the occurrence of gravity  
414 flow deposits during the late-stage sedimentation of the Taodonggou Group. The organic matter type in the mudstones during  
415 this period was influenced by gravity flows.

#### 416 **5.4 Formation mechanism of the Taodonggou Group mudstone**

417 Based on the sedimentary environment, provenance, and sedimentation mode during the deposition of the Taodonggou  
418 Group mudstones, this study has constructed the formation mechanism of the Taodonggou mudstones. The results indicate  
419 that the formation of the Taodonggou Group mudstones can be divided into three stages.

420 In the early of the Taodonggou Group, Bogda Mountain began to rise but did not emerge from the water surface. The  
421 sediment source is mainly from North Tianshan and Kelameili Mountain, and the secondary source area is Jueluotage  
422 Mountain in the south of the Turpan-Hami basin. The stratum of the Taodonggou Group was deposited in a warm and humid  
423 paleoclimate with high weathering intensity and a stable input of terrigenous detritus. In addition, the sedimentary water body  
424 is deep at this time, creating a deep lake environment of brackish water and dyoxic. However, this period inherited the gravity  
425 flow sedimentation characteristics from the Early Permian. Due to the influence of gravity flows, terrestrial organic matter  
426 was transported to the deep lake, resulting in the input of organic matter in the mudstones primarily derived from terrestrial  
427 higher plants (Miao et al., 2021). Consequently, a high-quality Type III organic matter source rock was formed (Fig.15a).

428 In the middle of the Taodonggou Group, with the continuous uplift of Bogda Mountain and hydrothermal activity, the  
429 climate changed into a hot and humid paleoclimate, the weathering degree further increased, and the input of terrigenous  
430 detritus increased. The provenance areas are Bogda Mountain and Jueluotage Mountain. In addition, during this period, the  
431 sedimentary center gradually transferred to the Taibei sag, and the sedimentary water body became shallow, which was a  
432 dyoxic intermediate-depth lake environment. Due to the nutrients brought by hydrothermal activities, the lower algae  
433 multiplied during this period, and the salinity of the sedimentary water body became lower, becoming a freshwater  
434 environment and thus depositing a set of high-quality II<sub>2</sub> organic source rocks.

435 In the late Taodonggou Group, the uplift of Bogda Mountain basically stopped, and the climate changed to a warm and  
436 humid paleoclimate again. The weathering degree was high, and the input of terrigenous debris was reduced. Bogda Mountain

437 and Jueluotage Mountain remained the provenance areas. The sedimentary center was essentially transferred to the Taibei Sag  
438 at this time. During this period, the salinity of the sedimentary water body was high, and the sedimentary water body became  
439 deeper. It was a deep lake environment with dyoxic and brackish water. During this period, the sedimentation was also  
440 influenced by gravity flows, leading to changes in lithology and organic matter type. As a result, the organic matter type in  
441 the mudstones deposited during this period transitioned to Type III.

## 442 **6 Conclusion**

443 Through the mineral composition and element geochemistry analysis of the Taodonggou Group mudstone, the following  
444 understandings have been obtained:

445 (1) The mudstone minerals of the Taodonggou Group are mainly clay and quartz and can be classified into 4 petrographic  
446 types according to their mineral fractions.

447 (2) The Taodonggou Group mudstone was deposited in an intermediate-depth or deep, dyoxic, freshwater-brackish lake  
448 environment under warm and humid paleoclimatic conditions. The input of terrestrial debris was stable, but the sedimentation  
449 rate was slow. In addition, the sedimentation in the middle stage was influenced by hydrothermal activities. In addition, the  
450 source rocks of the Taodonggou Group mudstone are mainly andesitic and feldspathic volcanic rocks. Sediment sorting and  
451 recycling were weak, and hydrocarbon source information was well preserved. The tectonic background of the source area  
452 was a continental island arc and an oceanic island arc.

453 (3) The sedimentary environment, sources, and sedimentary methods have significant impacts on the organic matter  
454 types of the Taodonggou Group. In the early taodonggou Group, the sedimentation center was in the Bogda area. At this time,  
455 the Bogda Mountain region was not exposed, and the depositional processes inherited the characteristics of Early Permian  
456 gravity flow sedimentation, resulting in the widespread deposition of a series of high-quality Type III source rocks in the  
457 basin. In the middle taodonggou Group, the sedimentation center gradually migrated to the Taibei Sag. During this period, the  
458 Bogda Mountain region experienced uplift and hydrothermal activity, and the depositional processes gradually transitioned  
459 to traction flows, resulting in the widespread deposition of a series of Type II source rocks in the basin. In the late taodonggou  
460 Group, the uplift of the Bogda Mountain region ceased, and the sedimentation center completely shifted to the Taibei Sag.  
461 Meanwhile, under the influence of gravity flows, the organic matter types of the Taodonggou mudstone changed to Type III.

## 462 **Data availability**

463 Data will be made available on request.

## 464 **Acknowledgement**

465 This study was supported by National Major Science and Technology Project of China (grant nos. 2016ZX05066001-  
466 002; 2017ZX05064-003-001; 2017ZX05035-02 and 2016ZX05034-001-05), Innovative Research Group Project of the  
467 National Natural Science Foundation of China (grant nos. 41872135 and 42072151), PetroChina Science and Technology

468 Project (grant nos. 2021DJ0602). We thank Hangzhou Yanqu Information Co., Ltd, Key Laboratory of natural gas  
469 accumulation, China National Petroleum Corporation and development and Beijing Orient Smart for providing testing  
470 samples and test equipments, as well as our colleagues' useful suggestions.

#### 471 **Author contribution**

472 Miao H. and Guo J.Y. designed experiments, Wang Y.B. and Jiang Z.X. revised the first draft of the manuscript, Guo J.  
473 Y., Wang Y.B. and Jiang Z.X. provided financial support, Miao H. and Zhang C.J. provided language services and figure  
474 production, Li C.M. investigated and revised the ideas of the article, and Miao H. prepared the manuscript with your  
475 contributions. All authors contributed to the review of the manuscript.

#### 476 **Competing interests**

477 The contact author has declared that none of the authors has any competing interests.

#### 478 **References**

- 479 Algeo, T.J., and Ingall, E.: Sedimentary Corg:P ratios, paleocean ventilation, and Phanerozoic atmospheric pO<sub>2</sub>. *Palaeogeogr.*  
480 *Palaeoclimatol. Palaeoecol.*, 256, 3–4, 130–155, 2007.
- 481 Algeo, T. J., and Maynard, J. B.: Trace-element behavior and redox facies in core shales of Upper Pennsylvanian Kansas-type  
482 cyclothems. *Chem. Geol.*, 206, 3-4, 289-318, 2004.
- 483 Allègre, C. J., and Minster, J. F.: Quantitative models of trace element behavior in magmatic processes. *Earth Planet. Sci.*  
484 *Lett.*, 38, 1–25, 1978.
- 485 Basu, A., Bickford, M. E., and Deasy, R.: Inferring tectonic provenance of siliciclastic rocks from their chemical compositions:  
486 A dissent. *Sediment. Geol.*, 336, 26–35, 2016.
- 487 Bhatia, M. R.: Plate tectonics and geochemical composition of sandstones. *J. Geol.*, 91, 611– 627, 1983.
- 488 Bhatia, M. R., and Crook, K. A. W.: Trace element characteristics of graywackes and tectonic setting discrimination of  
489 sedimentary basin. *Contrib. Mineral. Petrol.*, 92, 181–193, 1986.
- 490 Cai, Y. L., Ouyang, F., Luo, X. R., Zhang, Z. L., Wen, M. L., Luo, X. N., and Tang, R.: Geochemical Characteristics and  
491 Constraints on Provenance, Tectonic Setting, and Paleoweathering of Middle Jurassic Zhiluo Formation Sandstones in the  
492 Northwest Ordos Basin, North-Central China. *Minerals*, 12,5, 603, 2022.
- 493 Cao, L., Zhang, Z. H., Zhao, J. Z., Jin, X., Li, H., Li, J. Y., and Wei, X. D.: Discussion on the applicability of Th/U ratio for  
494 evaluating the paleoredox conditions of lacustrine basins. *Int. J. Coal geol.*, 248, 103868, 2021.
- 495 Cao, J., Yang, R. F., Yin, W., Hu, G., Bian, L. Z., and Fu, X. G.: Mechanism of Organic Matter Accumulation in Residual Bay  
496 Environments: The Early Cretaceous Qiangtang Basin, Tibet. *Energy & Fuels*, 32,2, 1024-1037, 2018.
- 497 Carroll, A., Graham, S., Hendrix, M., Ying, D., and Zhou, D.: Late Paleozoic tectonic amalgamation of northwestern China:  
498 sedimentary record of the northern Tarim, northwestern Turpan, and southern Junggar basins. *Geol. Soc. Am. Bull.*, 107, 5,



499 571-594, 1995.

500 Carroll, A., Liang, Y. H., Graham, S., Xiao, X. H., Hendrix, S., Chu, J. C., and McKnight, L.: Junggar basin, northwest China:  
501 trapped Late Paleozoic Ocean. *Tectonophysics*, 181, 1–14, 1990.

502 Chen, X., Niu, R.J., and Cheng, J.H.: The Sequence stratigraphy of Middle Permian-Triassic in Turpan-Hami Basin. *Xinjiang*  
503 *Pet. Geol.*, 24, 6, 494-497, 2003.

504 Deditius, A.: Arsenic Environmental Geochemistry, Mineralogy, and Microbiology. *Reviews in Mineralogy and Geochemistry*,  
505 vol 79. *Economic Geology*, 110, 7, 1905-1907, 2015.

506 Essefi, E.: Geochemistry and mineralogy of the sebka Oum El Khialate evaporites mixtures, southeastern Tunisia. *Resource*  
507 *Geology*, 71, 3, 242-249, 2021.

508 Floyd, P. A., Leveridge, B. E.: Tectonic environment of the Devonian Gramscatho Basin, South Cornwall: framework mode  
509 and geochemical evidence from turbiditic sandstones. *Journal of the Geological Society*, 144, 4, 531-542, 1987.

510 Gehrels, G. E., Valencia, V. A., and Ruiz, J.: Enhanced precision, accuracy, efficiency, and spatial resolution of U-Pb ages by  
511 laser ablation-multicollector-inductively coupled plasma-mass spectrometry. *Geochem., Geophys., Geosyst.*, 9, 3, 1–13, 2008.

512 Glaser, K. S., Miller, C. K., Johnson, G. M., Kleinberg, R. L., and Pennington, W. D.: Seeking the sweet spot: Reservoir and  
513 completion quality in organic shales. *Oilfield Review*, 25, 16–29, 2014.

514 Greene, T. J., Carroll, A. R., Wartes, M., Graham, S. A., and Wooden, J. L.: Integrated provenance analysis of a complex  
515 orogenic terrane: Mesozoic uplift of the Bogda Shan and inception of the Turpan-Hami Basin, NW China. *Journal of*  
516 *Sedimentary Research*, 75, 20, 251-267, 2005.

517 Guo, Z., Zhang, Z., Wu, C., Fang, S., and Zhang, R.: The Mesozoic and Cenozoic exhumation history of Tianshan and  
518 comparative studies to the Junggar and Altai mountains *Acta Geol. Sin.*: 80, 1, 1-15, 2006.

519 Hatch, J.R., and Leventhal, J.S.: Relationship between inferred redox potential of the depositional environment and  
520 geochemistry of the Upper Pennsylvanian (Missourian) Stark shale member of the Dennis Limestone, Wabaunsee County,  
521 Kansas, USA. *Chem. Geol.*, 99, 65–82, 1992.

522 Herkat, M., and Ladjal, A.: Paleobathymetry of foraminiferal assemblages from the Pliocene of the Western Sahel (North-  
523 Algeria). *Palaeogeography Palaeoclimatology* 374, 144-163, 2013.

524 Hu, F., Meng, Q., and Liu, Z.: Mineralogy and element geochemistry of oil shales in the Lower Cretaceous Qingshankou  
525 Formation of the southern Songliao Basin, northeast China: implications of provenance, tectonic setting, and  
526 paleoenvironment. *ACS Earth Space Chem.*, 5, 365–380, 2021.

527 Ji, H., Tao, H., Wang, Q., Qiu, Z., Ma, D., Qiu, J., and Liao P.: Early to middle Jurassic tectonic evolution of the Bogda  
528 mountains, northwest China: evidence from sedimentology and detrital zircon geochronology. *J. Asian Earth Sci.*, 153, 57-74,  
529 2018.

530 Jiang, S. H., Li, S. Z., Somerville, I. D., Lei, J. P., and Yang, H. Y.: Carboniferous-Permian tectonic evolution and sedimentation  
531 of the Turpan-Hami Basin, NW China: Implications for the closure of the Paleo-Asian Ocean. *J. Asian Earth Sci.*, 113, 644-  
532 655, 2015.

533 Kidder, D. L., and Erwin, D. H.: Secular distribution of biogenic silica through the phanerozoic: Comparison of silica-replaced  
534 fossils and bedded cherts at the series level. *J. GEOL.*, 109, 4, 509-522, 2001.

535 Korobkin, V. V., and Buslov, M. M.: Tectonics and geodynamics of the western Central Asian Fold Belt (Kazakhstan  
536 Paleozoides). *Russian Geology and Geophysics*, 52, 12, 1600-1618, 2011.

537 Kröner, S. R., and McLennan, S. M.: *The Continental Crust: Its Composition and Evolution*; Blackwell: Oxford, 312, 1985.

538 Kroonenberg, S.B.: Effect of provenance, sorting and weathering on the geochemistry of fluvial sands from different tectonic  
539 and climatic environments. In *Proceedings of the 29th International Geological Congress, Part A, Kyoto, Japan, 24 August–*  
540 *3 September*, 69, 81, 1992.

541 Lerman, A., and Baccini, P.: *Lakes: Chemistry, Geology, Physics*. Springer-Verlag, New York, 1978.

542 Li, C. M., Liu, J. T., Ni, L. B., and Fan, S. W.: Characteristics of deep geological structure and petroleum exploration prospect  
543 in Turpan-Hami Basin. *China Petroleum Exploration*, 26, 4, 44-57, 2021. (In Chinese with English abstract)

544 Li, L., Qu, Y.Q., Meng, Q.R., and Wu, G.L.: Gravity Flow Sedimentation: Theoretical Studies and Field Identification. *Acta*  
545 *Sedimentologica Sinica*, 29,4, 677-688, 2011.

546 Li, RB.: Filling characteristic and research significance of Permian in Tainan Depression of Tuha Basin. *J. Jilin University*  
547 *(Earth science Edition)* 49, 6, 1518-1528, 2019.

548 Li, Y. J., Sun, P. C., Liu, Z. J., Yao, S. Q., Xu, Y. B., and Liu, R.: Geochemistry of the Permian Oil Shale in the Northern  
549 Bogda Mountain, Junggar Basin, Northwest China: Implications for Weathering, Provenance, and Tectonic Setting. *ACS Earth*  
550 *and Space Chemistry* 4, 8, 1332-1348, 2020.

551 Li, Y. L., Shan, X., Gelwick, K. D., Yu, X. H., Jin, L. N., Yao, Z. Q., Li, S. L., and Yang, S. Y.: Permian mountain building in  
552 the bogda mountains of NW China. *International Geology Review*, 2048270, 2022.

553 Li, W., Hu, J., Li, D., Liu, J., Sun, Y., and Liang, J.: Analysis of the late Paleozoic and Mesozoic paleocurrents and its  
554 constructional significance of the northern Bogdashan, Xinjiang. *Acta Sedimentol. Sin.*, 25,2, 283-292, 2007.

555 Liu, D., Zhang, C., Yao, E., Song, Y., Jiang, Z., and Luo, Q.: What generated the Late Permian to Triassic unconformities in  
556 the southern Junggar Basin and western Turpan Basin; tectonic uplift, or increasing aridity? *Palaeogeogr. Palaeoclimatol.*  
557 *Palaeoecol.*, 468, 1-17, 2017.

558 Liu, D., Kong, X., Zhang, C., Wang, J., Yang, D., Liu, X., Wang, X., and Song, Y.: Provenance and geochemistry of Lower to  
559 Middle Permian strata in the southern Junggar and Turpan basins: a terrestrial record from mid-latitude NE Pangea.  
560 *Palaeogeogr. Palaeoclimatol. Palaeoecol.*, 495, 259-277, 2018.

561 Liu, G., Zhou, D.: Application of microelements analysis in identifying sedimentary environment-taking Qianjiang Formation  
562 in the Jiang Han Basin as a example. *Pet. Geo. Exp.* 29,3, 307-311,2007. (In Chinese with English abstract)

563 Maravelis, A. G., Offler, R., Pantopoulos, G., and Collins, W. J.: Provenance and tectonic setting of the Early Permian  
564 sedimentary succession in the southern edge of the Sydney Basin, eastern Australia. *Geological J.* 56, 4, 2258-2276, 2021.

565 McLennan, S. M., Hemming, S., McDaniel, D. K., and Hanson, G.N.: Geochemical approaches to sedimentation, provenance,  
566 and tectonics. *Spec. Pap. Geol. Soc. Am.* 284, 21–40, 1993.

567 McLennan, S. M., Taylor, S. R., and Kröner, A.: Geochemical evolution of Archean shales from South Africa I: The Swaziland  
568 and Ponggola Supergroups. *Precambrian Res.*, 22, 93– 124, 1983.

569 Mei, X., Li, X.J., Mi, P.P., Zhao, L., Wang, Z.B., Zhong, H.X., Yang, H., Huang, X.T, He, M.Y., Xiong, W., and Zhang, Y.:  
570 Distribution regularity and sedimentary differentiation patterns of China seas surface sediments. *Geology in China*, 47,5,1447-  
571 1462, 2020. (In Chinese with English abstract)

572 Miao, H., Wang, Y. B., Guo, J. Y., Fu, Y., and Li, J. H.: Weathering correction and hydrocarbon generation and expulsion  
573 potential of Taodonggou Group source rocks in Taibei Sag in Turpan-Hami Basin. *Petroleum Geology & Oilfield*  
574 *Development in Daqing*, 42,2, 22-32, 2023.

575 Miao, H., Wang, Y. B., Guo, J. Y., Han, W. L., and Gong, X.: Evaluation of Middle Permian source rocks of the Taodonggou  
576 Group in the Turpan Hami Basin. *Geophysical Prospecting for Petroleum*, 61, 4, 733-742, 2022. (In Chinese with English  
577 abstract)

578 Miao, H., Wang, Y. B., He, C., Li, J. H., Zhang, W., Zhang, Y. J., and Gong, X.: Fault development characteristics and reservoir  
579 control in Chengbei fault step zone, Bohai Bay Basin. *Lithologic Reservoirs*, 34, 2, 105-115, 2022a. (In Chinese with an  
580 English abstract).

581 Miao, H., Wang, Y. B., Ma, Z. T., Guo, J. Y., and Zhang, Y. J.: Generalized Deltalog R model with spontaneous potential and  
582 its application in predicting total organ carbon content. *Journal of Mining Science and Technology*, 7, 4, 417-426, 2022b. (In  
583 Chinese with English abstract)

584 Miao, H., Wang, Y. B., Zhao, S. H., Guo, J. Y., Ni, X. M., Gong, X, Zhang, Y. J., and Li, J. H.: Geochemistry and Organic  
585 Petrology of Middle Per-mian Source Rocks in Taibei Sag, Turpan-Hami Basin, China: Implication for Organic Matter  
586 Enrichment. *ACS Omega*, 6,47, 31578-31594, 2021.

587 Miao, J. Y., Zhou, L. F., Deng, K., Li, J. F., Han, Z. Y., and Bu, Z. Q.: Organic Matters from Middle Permian Source rocks of  
588 Northern Xinjiang and Their Relationships with Sedimentary environments. *Geochemica*, 6,551-560, 2004. (In Chinese with  
589 English abstract)

590 Nesbitt, H. W., and Young, G. M.: Prediction of some weathering trends of plutonic and volcanic rocks based on  
591 thermodynamic and kinetic considerations. *Geochim. Cosmochim. Acta.*, 48, 7, 1523-1534, 1984.

592 Novikov, I. S.: Reconstructing the stages of orogeny around the Junggar basin from the lithostratigraphy of Late Paleozoic,  
593 Mesozoic, and Cenozoic sediments. *Russian Geology and Geophysics*. 54, 2, 138-152, 2013.

594 Obrist-Farner, J., Yang, W., and Hu, X. F.: Nonmarine time-stratigraphy in a rift setting: an example from the Mid-Permian  
595 lower Quanzijie low-order cycle Bogda Mountains, NW China. *J. Palaeogeogr.*, 4, 1, 27-51, 2015.

596 Pinto, L., Munoz, C., Nalpas, T., and Charrier, R.: Role of sedimentation during basin inversion in analogue modelling. *Journal*  
597 *of Structural Geology*, 32, 4, 554-565, 2010.

598 Rollinson, H. R.: *Using Geochemical Data: Evaluation, Presentation, Interpretation*; Longman Scientific Technical: New York,  
599 1993.

600 Rosenthal, Y., Lam, P., Boyle, E. A., and Thomson, J.: Authigenic cadmium enrichments in suboxic sediments: precipitation  
601 and postdepositional mobility - sciencedirect. *Earth & Planetary Science Letters*, 132, 1-4, 99-111, 1995.

602 Roser, B. P., Korsch, R. J.: Provenance Signatures of Sandstone-mudstone suites determined using discriminant function  
603 analysis of major-element data. *Chem. Geol.* 67, 119– 139, 1988.

604 Ross, D.J.K., and Bustin, R. M.: Investigating the use of sedimentary geochemical proxies for paleoenvironment interpretation  
605 of thermally mature organic-rich strata: Examples from the Devonian–Mississippian shales, Western Canadian Sedimentary  
606 Basin. *Chem. Geol.*, 260, 1–19, 2009

607 Schoepfer, S. D., Shen, J., Wei, H. Y., Tyson, R. V., Ingall, E., and Algeo, T. J.: Total organic carbon, organic phosphorus, and  
608 biogenic barium fluxes as proxies for paleomarine productivity. *Earth Sci. Rev.*, 149, 23–52, 2015.

609 Shao, L., Li, W.H., and Yuan, M.S.: Characteristic of sandstone and its tectonic implications of the Turpan Basin. *Acta*  
610 *Sedimentologica Sinica*, 17,3, 435–441, 1999.

611 Shao, L., Stattegger, K., and Garbe-Schoenberg, C.: Sandstone petrology and geochemistry of the Turpan Basin (NW China):  
612 implications for the tectonic evolution of a Continental Basin. *Journal of Sedimentary Research*, 71, 1, 37–49,2001. (In  
613 Chinese with English abstract)

614 Shi, J., Zou, Y. R., Cai, Y. L., Zhan, Z. W., Sun, J. N., Liang, T., and Peng, P. A.: Organic matter enrichment of the Chang 7  
615 member in the Ordos Basin: Insights from chemometrics and element geochemistry. *Marine Petroleum Geology*, 134, 105306,  
616 2021.

617 Shi, Y. Q, Ji, H. C., Yu, J. W, Xiang, P. F., Yang, Z. B, and Liu, D. D.: Provenance and sedimentary evolution from the Middle  
618 Permian to Early Triassic around the Bogda Mountain, NW China: A tectonic inversion responding to the consolidation of  
619 Pangea. *Mar. Pet. Geol.*, 114, 104169, 2020.

620 Shu, L., Wang, B., Zhu, W., Guo, Z., Charvet, J., and Zhang, Y.: Timing of initiation of extension in the Tianshan, based on  
621 structural, geochemical and geochronological analyses of bimodal volcanism and olistostrome in the Bogda Shan (NW China).  
622 *Int. J. Earth Sci.*, 100, 7, 1647-1663, 2011.

623 Song, J., Bao, Z., Zhao, X. M., Gao, Y. S., Song, X. M., Zhu, Y. Z., Deng, J., Liu, W., Wang, Z. C., Ming, C. D., Meng, Q. K.,  
624 Zhang, L., Mao, S. W., Zhang, Y. L., Yu, X., and Wei, M. Y.: Sedimentology and geochemistry of Middle–Upper Permian in  
625 northwestern Turpan–Hami Basin, China: Implication for depositional environments and petroleum geology. *Energy*  
626 *Exploration & Exploitation* 36, 4, 910-941, 2018.

627 Sun, G., and Liu, Y.: The preliminary analysis of the uplift time of Bogda Mountain, Xinjiang, Northwest China. *Acta*  
628 *Sedimentol. Sin.*, 27, 3, 487-491, 2009.

629 Tang, W., Zhang, Z., Li, J., Li, K., Chen, Y., and Guo, Z.: Late Paleozoic to Jurassic tectonic evolution of the Bogda area  
630 (northwest China): evidence from detrital zircon U–Pb geochronology. *Tectonophysics*, 626, 144-156, 2014.

631 Taylor, S. R., and McLennan, S. M.: *The continental crust: Its composition and evolution*. Blackwell Science Publications,  
632 Oxford. 1985.

633 Thorpe, C. L., Law, G. T. W., Boothman, C., Lloyd, J. R., Burke, I. T., and Morris, K.: The Synergistic Effects of High Nitrate  
634 Concentrations on Sediment Bioreduction. *Geomicrobiol. J.*, 29, 5, 484-493, 2012.

635 Tian, J.Q., Liu, J.Z., Zhang, Z.B., and Cong, F.Y.: Hydrocarbon-generating potential, depositional environments, and  
636 organisms of the Middle Permian Tarlong Formation in the Turpan-Hami Basin, northwestern China. *GSA Bulletin* 129, 9-  
637 10, 1252–1265, 2017.

638 Tribouillard, N., Algeo, T. J., Baudin, F., and Riboulleau, A.: Analysis of marine environmental conditions based on  
639 molybdenum–uranium covariation—applications to Mesozoic paleoceanography. *Chem. Geol.* 324,46–58, 2012.

640 Tribouillard, N., Algeo, T. J., Lyons, T., and Riboulleau, A.: Trace metals as paleoredox and paleoproductivity proxies: an  
641 update. *Chemical Geology* 232, 1–2, 12–32, 2006.

642 Tribouillard, N. P., Desprairies, A., Lallier-verges, E., Bertrand, P., Moureau, N., Ramdani, A., and Ramanampiso, L.:  
643 Geochemical study of organic-matter rich cycles from the Kimmeridge Clay Formation of Yorkshire (UK): productivity versus  
644 anoxia. *Palaeogeography, Palaeoclimatology, Palaeoecology*, 108,1-2,165-181, 1994.

645 Warts, M. A., Carroll, A. R., and Greene, T. J.: Permian sedimentary record of the Turpan-Hami basin and adjacent regions,  
646 northwest China: Constraints on postamalgamation tectonic evolution. *Geological Society of America Bulletin*, 114,2, 131-  
647 152, 2002.

648 Wang, A., Wang, Z., Liu, J., Xu, N., Li, H.: The Sr/Ba ratio response to salinity in clastic sediments of the Yangtze River Delta.  
649 *Chem. Geol.*, 559, 119923, 2021.

650 Wang, L.: Sediment flux and mechanism for the uplifting of the mountain system around the Junggar inland basin Sediment.  
651 *Geol. Tethyan Geol.*, 16, 3, 39-46, 1996.

652 Wang, J., Cao, Y. C., Wang, X. T., Liu, K. Y., Wang, Z. K., and Xu, Q. S.: Sedimentological constraints on the initial uplift of  
653 the West Bogda Mountains in Mid-Permian. *Sci. Rep.* 8, 1453, 2018.

654 Wang, J., Wu, C., Li, Z., Zhu, W., Zhou, T., Wu, J., and Wang, J.: The tectonic evolution of the Bogda region from Late  
655 Carboniferous to Triassic time: evidence from detrital zircon U–Pb geochronology and sandstone petrography. *Geol. Mag.*,  
656 155, 5, 1063-1088, 2018.

657 Wang, J., Wu, C., Zhou, T., Zhu, W., Zhou, Y., Jiang, X., and Yang, D.: Source-to-Sink analysis of a transtensional rift Basin  
658 from syn-rift to uplift stages. *J. Sediment. Res.* 89, 4, 335-352, 2019.

659 Wang, J. L., Wu, C. D., Zhou, T. Q., Zhu, W., Li, X. Y., and Zhang, T.: Source and sink evolution of a Permian–Triassic rift–  
660 drift basin in the southern Central Asian Orogenic Belt: Perspectives on sedimentary geochemistry and heavy mineral analysis.  
661 *Journal of Asian Earth Sciences* 181, 103905, 2019.

662 Wang, Y.: Mixed Sedimentary Characteristics and Pattern of the Fan Delta in the Middle Permian Taerlanggou  
663 Profile, Xinjiang Province *Acta Sedimentologica Sinica*, 37, 5, 922-933, 2019. (In Chinese with English abstract)

664 Wang, Z. W., Yu, F., Wang, J., Fu, X. G., Chen, W. B., Zeng, S. Q., and Song, C. Y.: Palaeoenvironment evolution and organic  
665 matter accumulation of the Upper Triassic mudstone from the eastern Qiangtang Basin (Tibet), eastern Tethys. *Marine and*  
666 *Petroleum Geology* 130, 105113, 2021.

667 Wronkiewicz, D. J., and Condie, K. C.: Geochemistry of archean shales from the witwatersrand supergroup, south Africa:  
668 Source-area weathering and provenance. *Geochimica Cosmochimica Acta* 51, 9, 2401-2416, 1987.

669 Wei, H., Chen, D. Z., Wang, J. G., Yu, H., and Tucker, M. E.: Organic accumulation in the lower Chihhsia Formation (Middle  
670 Permian) of South China: Constraints from pyrite morphology and multiple geochemical proxies. *Palaeogeogr. Palaeoclimatol.*  
671 *Palaeoecol.*, 353, 73-86, 2012.

672 Wei, X.X.: Middle-Late Permian fossil woods from Northern Tuha Basin: Implications for Palaeoclimate. MS thesis, Wuhan:  
673 China university of Geosciences, 2015. (In Chinese with English abstract)

674 Wu, C., Li, H. W., Sheng, S. Z., Chen, T., Shi, X. F., and Jiang, M. L.: Characteristics and main controlling factors of  
675 hydrocarbon accumulation of Permian-Triassic in Lukeqin structural zone, Tuha Basin. *China Petroleum Exploration* 26, 4,  
676 137-148, 2021. (In Chinese with English abstract)

677 Xiong, X. H., and Xiao, J. F.: Geochemical Indicators of Sedimentary Environments—A Summary. *Earth and Environment*  
678 39, 3, 405-414, 2011. (In Chinese with English abstract)

679 Xu, C., Shan, X. L., Lin, H. M., Hao, G. L., Liu, P., Wang, X. D., Shen, M. R., Rexiti, Y., Li, K., Li, Z. S., Wang, X. M., Du,  
680 X. D., Zhang, Z.W., Jia, P. M., and He, W. T.: The formation of early Eocene organic-rich mudstone in the western Pearl River  
681 Mouth Basin, South China: Insight from paleoclimate and hydrothermal activity. *International Journal of Coal geology* 253,  
682 103957, 2022.

683 Xu, H.Y.: Characteristics of Permian Dark Fine-Grained Sedimentary rocks and their shale oil and gas Significance in the  
684 Northern Margin of Turpan-Hami Basin. MS thesis, Xi'an: Chang'an University, 2022. (In Chinese with English abstract)

685 Yang, Y., Song, C., and He, S.: Jurassic tectonostratigraphic evolution of the Junggar basin, NW China: a record of Mesozoic  
686 intraplate deformation in Central Asia. *Tectonics* 34, 1, 86-115, 2015.

687 Yang, W., Feng, Q., Liu, Y.Q., Tabor, N., Miggins, D., Crowley, J.L., Lin, J.Y., and Thomas, S.: Depositional environments  
688 and cyclo- and chronostratigraphy of uppermost Carboniferous–Lower Triassic fluvial–lacustrine deposits, southern Bogda  
689 Mountains, NW China — A terrestrial paleoclimatic record of mid-latitude NE Pangea. *Global and Planetary Change*, 73,  
690 2010, 15-113, 2010.

691 You, J., Liu, Y., Zhou, D., Zheng, Q., Vasichenko, K., and Chen, Z.: Activity of hydrothermal fluid at the bottom of a lake and  
692 its influence on the development of high-quality source rocks: Triassic Yanchang Formation, southern Ordos Basin, China.  
693 *Australian Journal of Earth Sciences* 67, 1, 115-128, 2019.

694 Yu, Y., Cai, H.L., Yin, T.J., Zhang, X.Q., Xu, H., Huang, Y.R., and Cao, T.T.: Sedimentary Characteristics and Depositional  
695 Model of Lacustrine Gravity Flow Deposits: A case study of the Cretaceous Pointe Indienne Formation of Block A, Lower  
696 Congo Basin. *Acta Sedimentologica Sinica*, 2022, 40, 1, 34-46, 2022.

697 Zhang, C., He, D., Wu, X., Shi, X., Luo, J., Wang, B., Yang, G, Guan, S., and Zhao, X.: Formation and evolution of multicycle  
698 superimposed basins in Junggar Basin. *China Petrol. Exp.*, 11, 1, 47-58, 2006.

699 Zhang, K., Song, Y., Jiang, S., Jiang, Z. X., Jia, C. Z., Huang, Y. Z., Wen, M., Liu, W. W., Xie, X. L., Liu, T. L., Wang, P. F.,  
700 Shan, C. A., and Wu, Y. H.: Mechanism analysis of organic matter enrichment in different sedimentary backgrounds: A case  
701 study of the Lower Cambrian and the Upper Ordovician–Lower Silurian, in Yangtze region. *Mar. Petrol. Geol.*, 99, 488–497,  
702 2019.

703 Zhang, S., Liu, C., Bai, J., Wang, J., Ma, M., Guan, Y., and Peng, H.: Provenance variability of the Triassic strata in the  
704 Turpan-Hami basin: detrital zircon record of Indosinian tectonic reactivation in eastern Tianshan. *Acta Geol. Sin.* 93, 6, 1850-  
705 1868, 2019.

706 Zhang, S. C., Zhang, B. M., Bian, L. C., Jing, Z. J., Wang, D. R., Zhang, X. Y., Gao, Z. Y., and Chen, J. F.: Development  
707 constraints of marine source rocks in China. *Earth Sci. Frontiers* 12, 3, 39-48, 2005. (In Chinese with English abstract)

708 Zhao, R., Zhang, J. Y., Zhou, C. M., Zhang, Z. J., Chen, S., Stockli, D.F., Olariu, C., Steel, R., and Wang, H.: Tectonic evolution  
709 of Tianshan-Bogda-Kelameili mountains, clastic wedge basin infill and chronostratigraphic divisions in the source-to-sink  
710 systems of Permian–Jurassic, southern Junggar Basin. *Mar. Petrol. Geol.* 114, 104200, 2020.

711 Zhao, B. S., Li, R. X., Qin, X. L., Wang, N., Zhou, W., Khaled, A., Zhao, D., Zhang, Y. N., Wu, X. L., and Liu, Q.:  
712 Geochemical characteristics and mechanism of organic matter accumulation of marine-continental transitional shale of the  
713 lower permian Shanxi Formation, southeastern Ordos Basin, north China. *Journal of Petroleum Science and Engineering*, 205,  
714 108815, 2021.

715 Zhu, Q. M., Lu, L. F., Pan A. Y., Tao, J. Y., Ding, J. H., Liu, W. L., and Li, M. W.: Sedimentary environment and organic

716 matter enrichment of the Lower Cambrian Niutitang Formation shale, western Hunan Province, China. *Petroleum Geology*  
717 & Experiment 43, 5, 797-854, 2021. (In Chinese with English abstract)

718 Zhu, X., Wang, B, Chen, Y., and Liu, H. S.: Constraining the Intracontinental Tectonics of the SW Central Asian Orogenic  
719 Belt by the Early Permian Paleomagnetic Pole for the Turfan-Hami Block. *Journal of Geophysical Research-solid earth*, 124,  
720 12, 12366-12387, 2019.



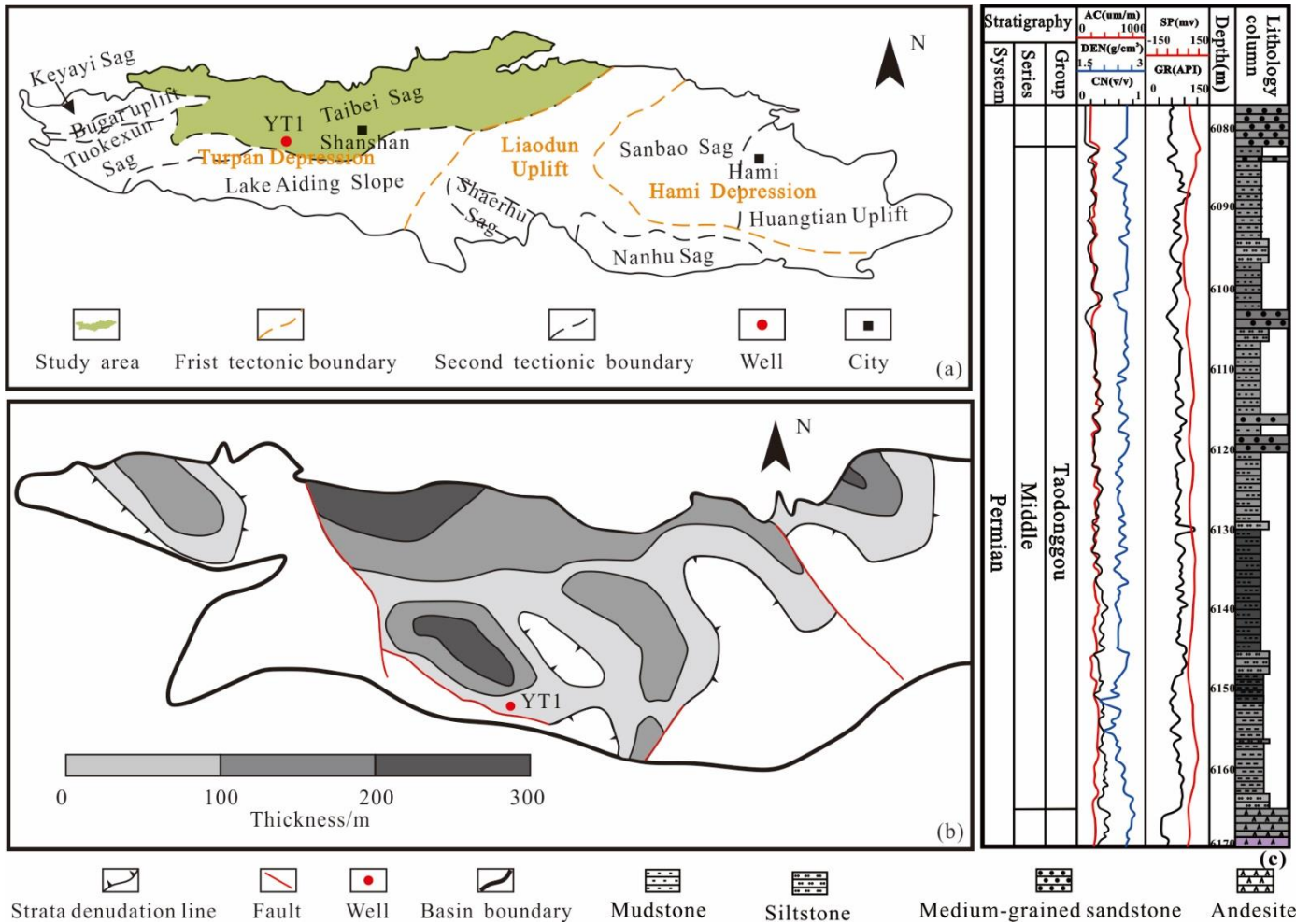


**Figure 1: Geological overview of the study area (modified after Miao et al., 2021; Miao et al., 2023): (a) Geological background of Turpan-Hami basin; (b) Thickness contour map of Taodonggou Group mudstone in Taibei sag; (c) YT1 stratum of Taodonggou Group**

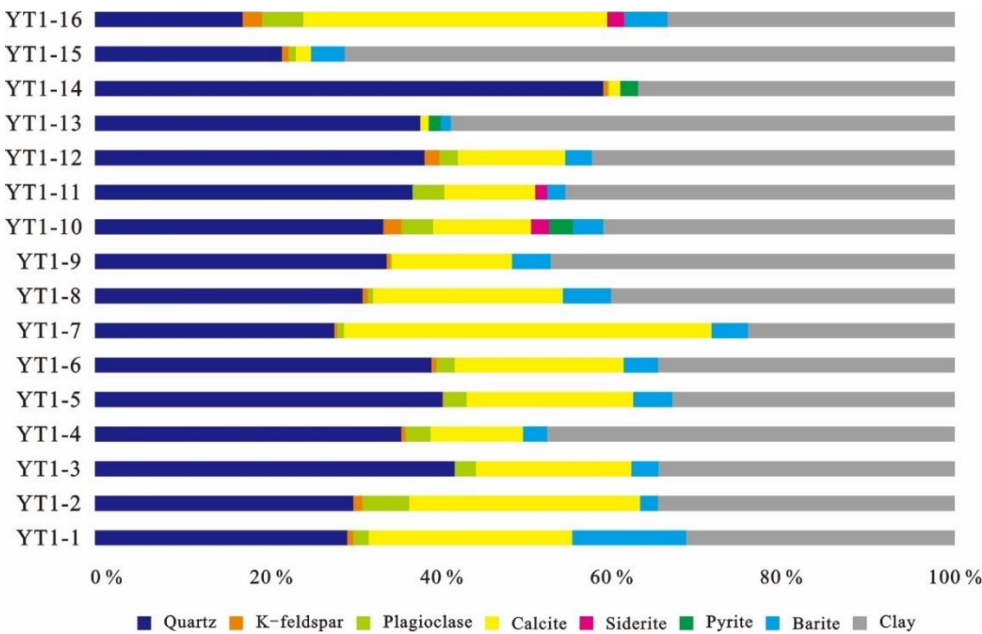
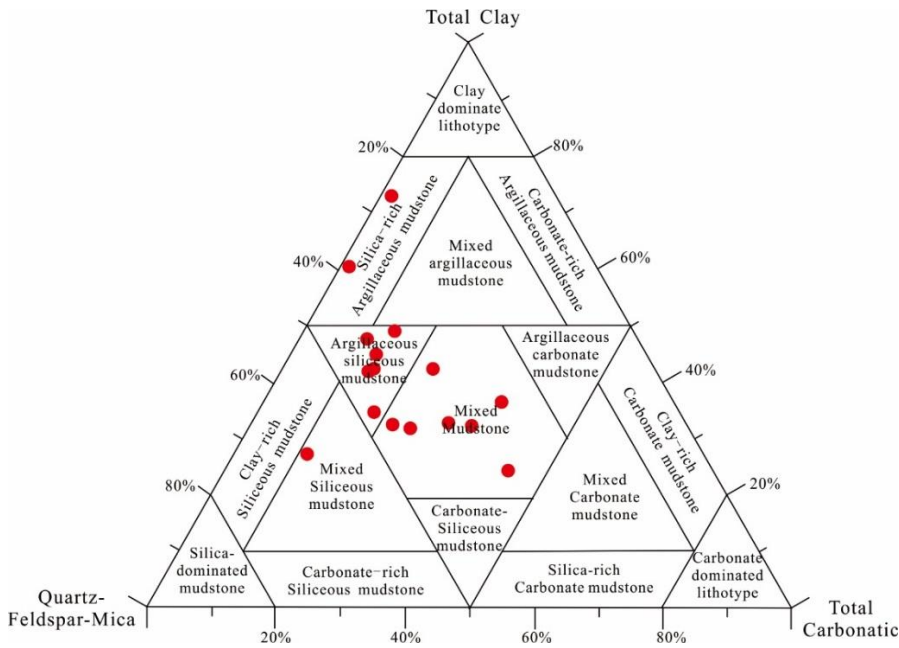
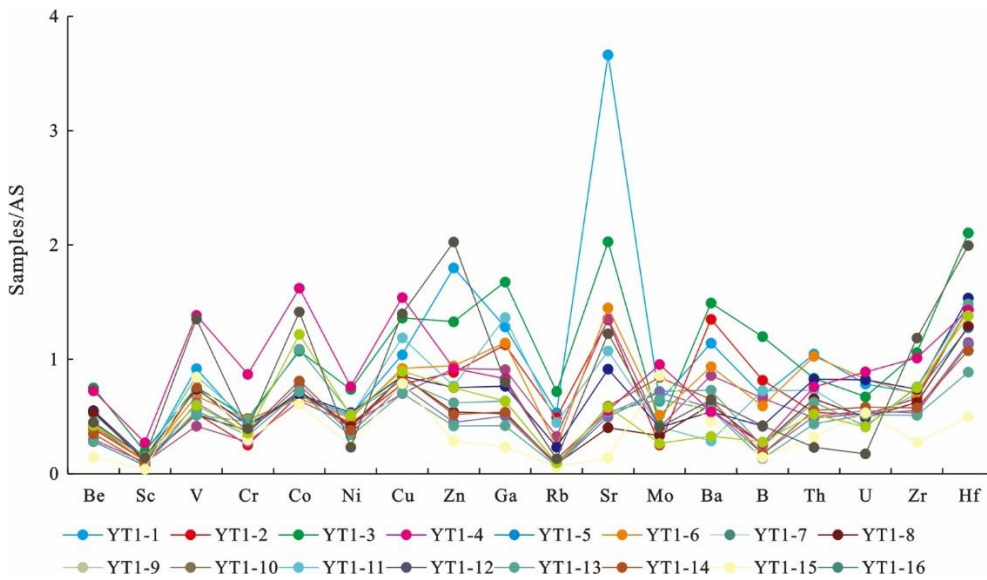


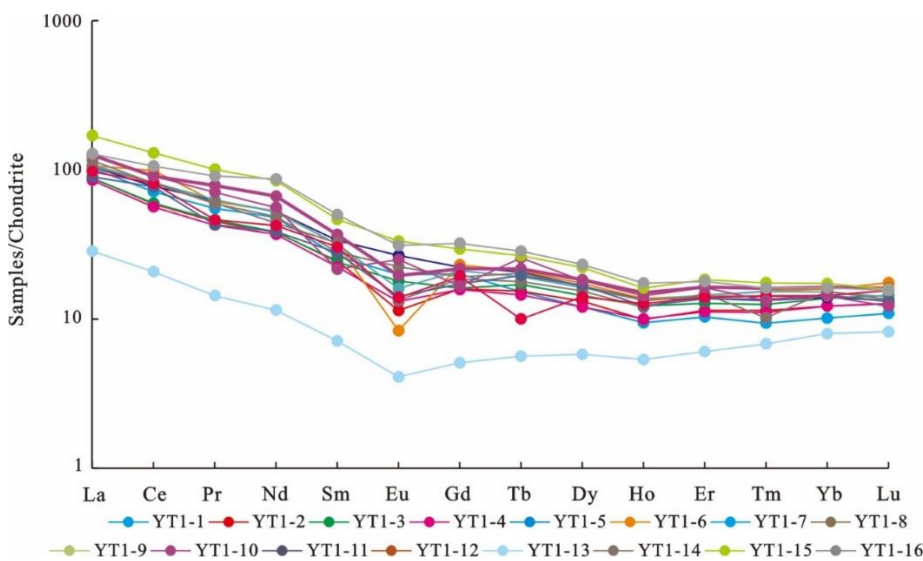
**Figure 2: Mineral composition of Taodonggou group mudstone in YT1 well**



726  
727 **Figure 3: Lithofacies classification of Taodonggou Group mudstone in well YT1(modified from Glaser et al., 2014)**



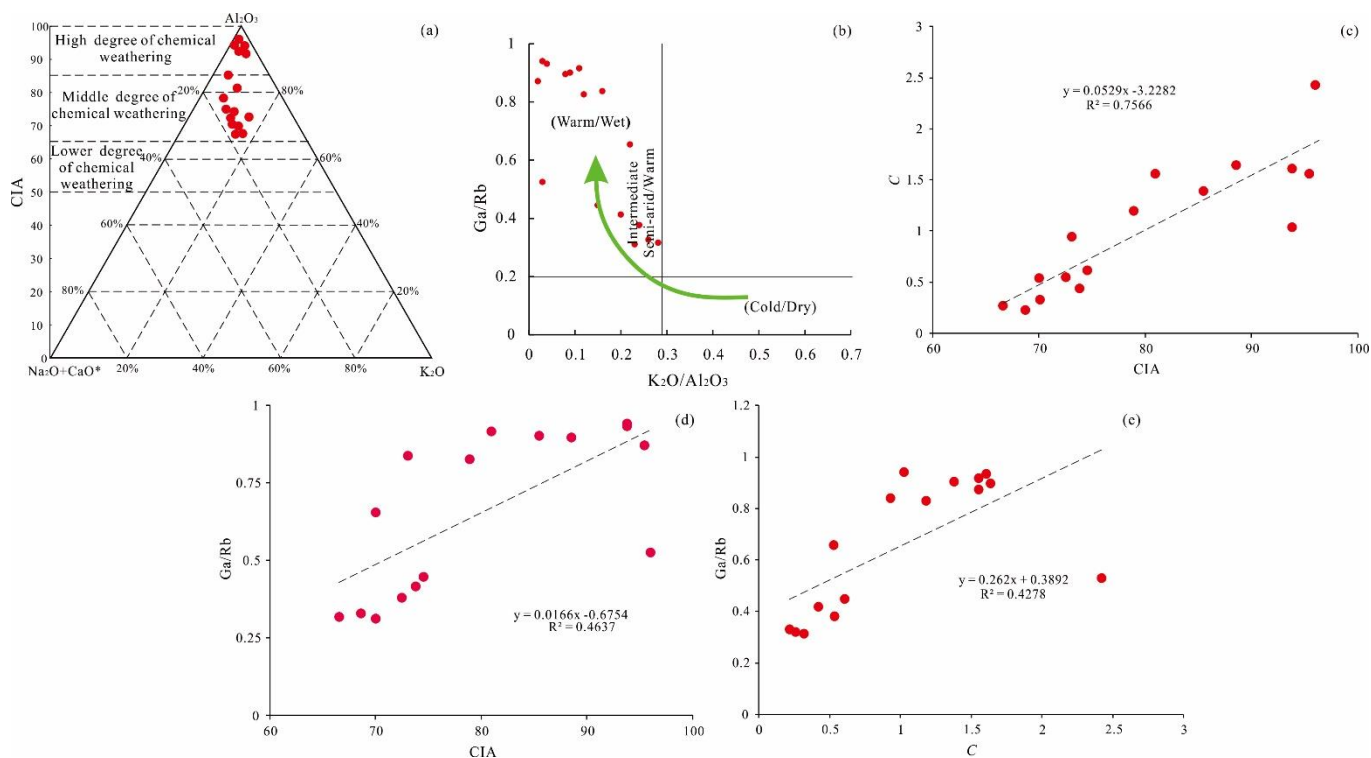
728  
729 **Figure 4: AS standardized multi-element diagrams of Taodonggou Group mudstone in the study area.**



730

731

**Figure 5: Standardized map of rare-earth element chondrite in mudstone of Taodonggou Group**



732

733

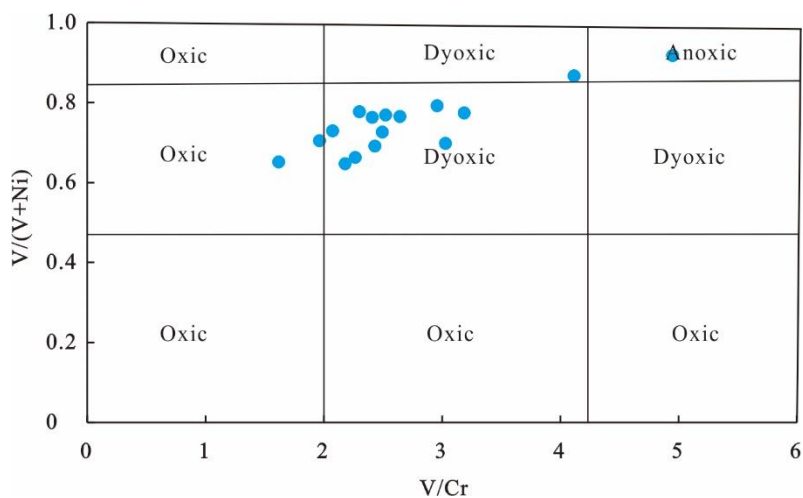
**Figure 6: Paleoclimate of Taodonggou Group: (a) CIA Characteristics of Taodonggou Group mudstone (modified from Nesbitt and Young,**

734

**1984); (b) cross plot of  $K_2O/Al_2O_3$  and  $Ga/Rb$  (modified from Roy and Roser, 2013); (c) cross plot of CIA and  $C$ ; (d) cross plot of CIA and**

735

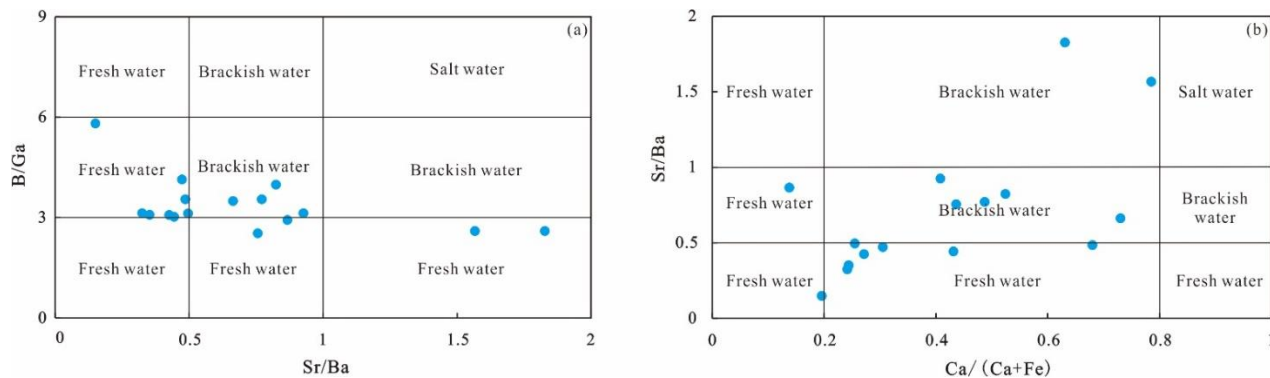
**$Ga/Rb$ ; (e) cross plot of  $C$  and  $Ga/Rb$**



736

737

**Figure 7: Cross plot of  $V/Cr$  and  $V/(V+Ni)$**



738

739

**Figure 8: Cross plot of  $B/Ga$  and  $Sr/Ba$  (a) and cross plot of  $Ca/(Ca+Fe)$  and  $Sr/Ba$  (b)**

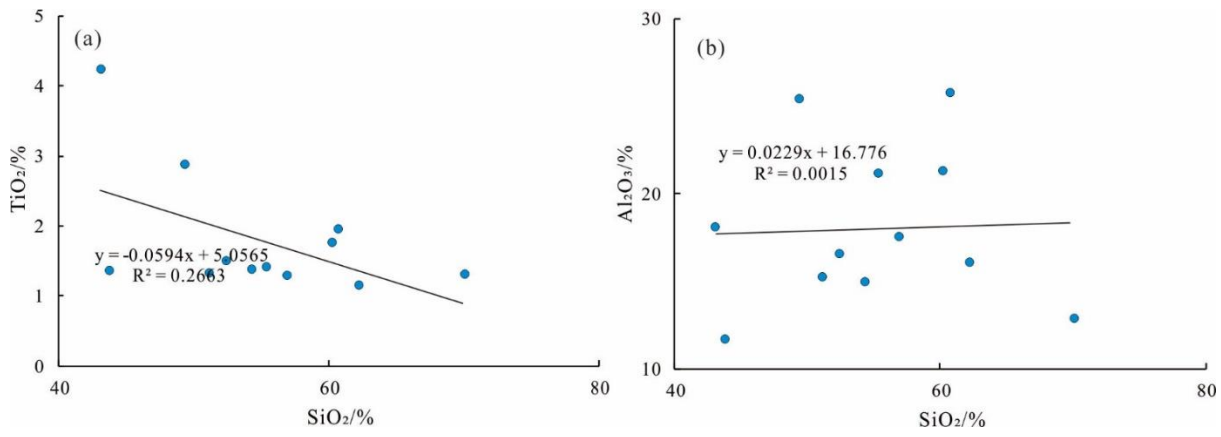


Figure 9: Intersection diagram of  $TiO_2$  and  $SiO_2$  (a) and intersection diagram of  $Al_2O_3$  and  $SiO_2$  (b)

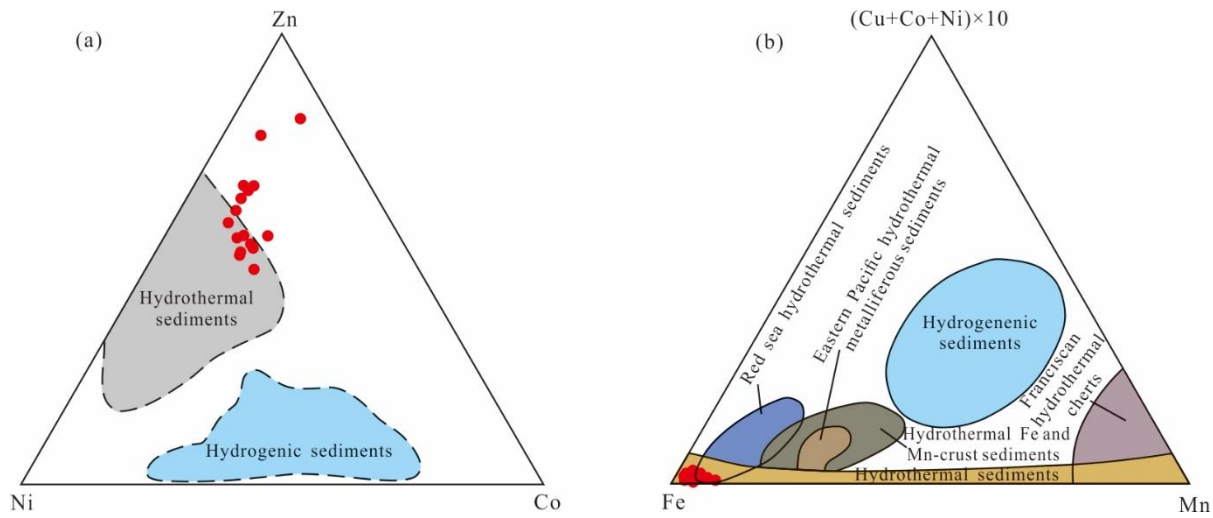
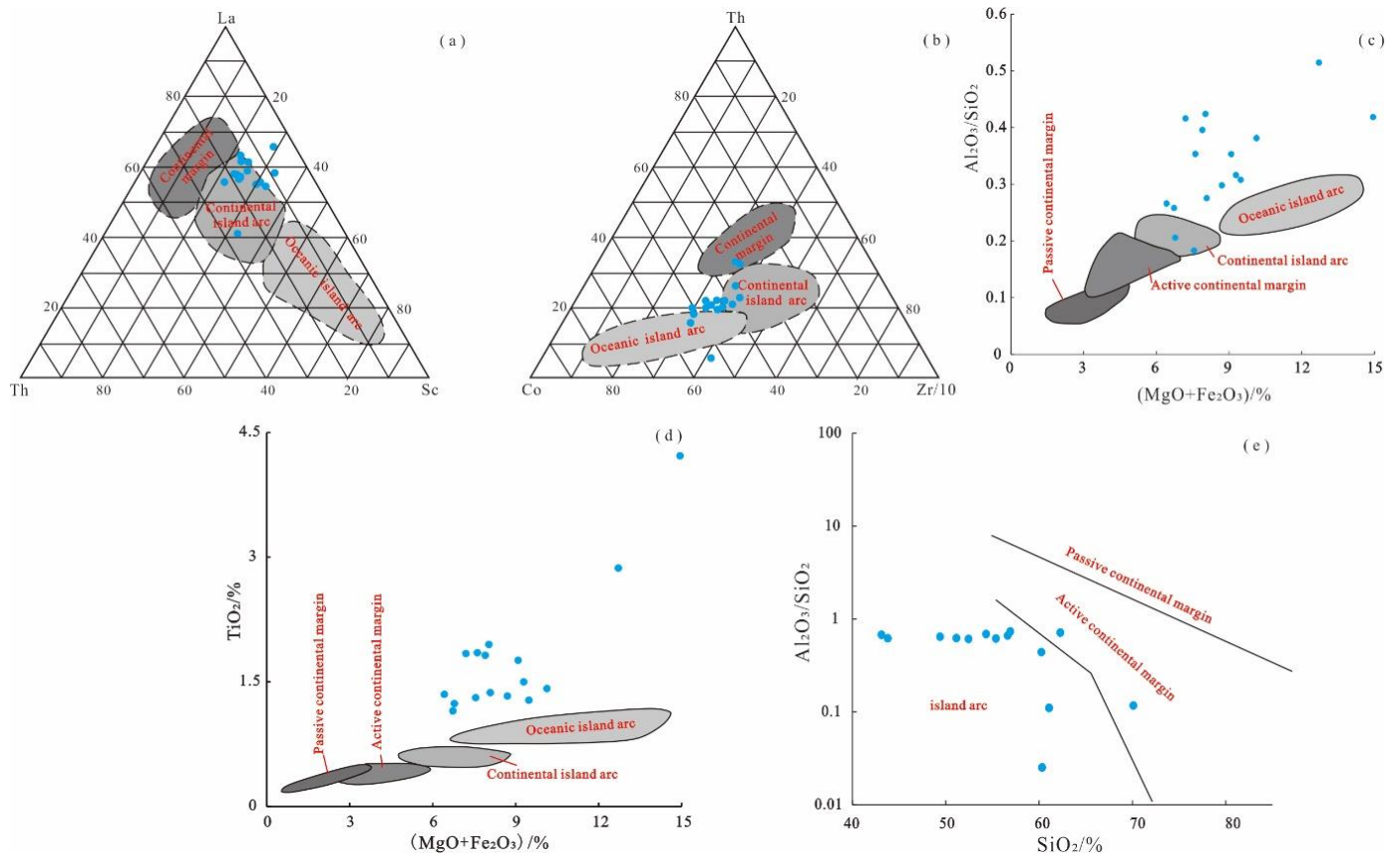
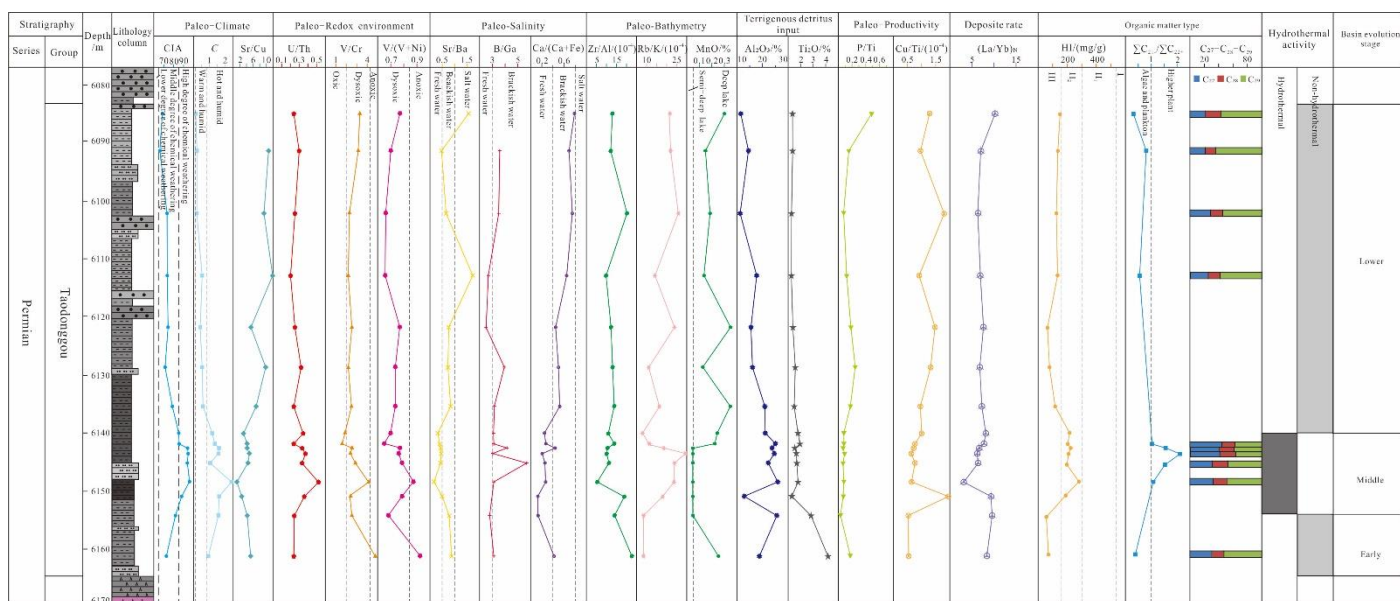


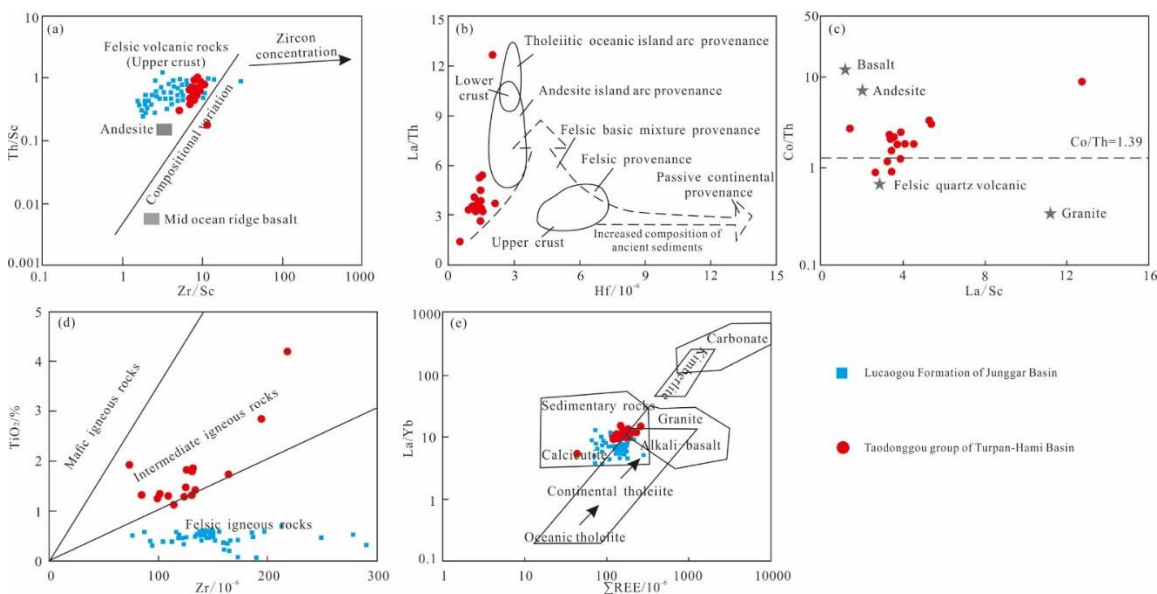
Figure 10: Zn-Ni-Co ternary diagram (a) and  $(Cu+Co+Ni) \times 10$ -Fe-Mn ternary diagram (b) (modified after You et al., 2019)



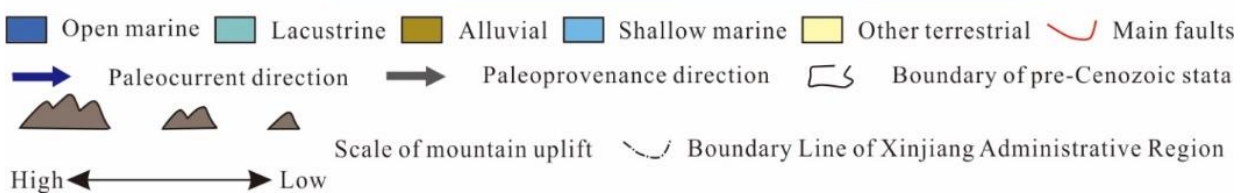
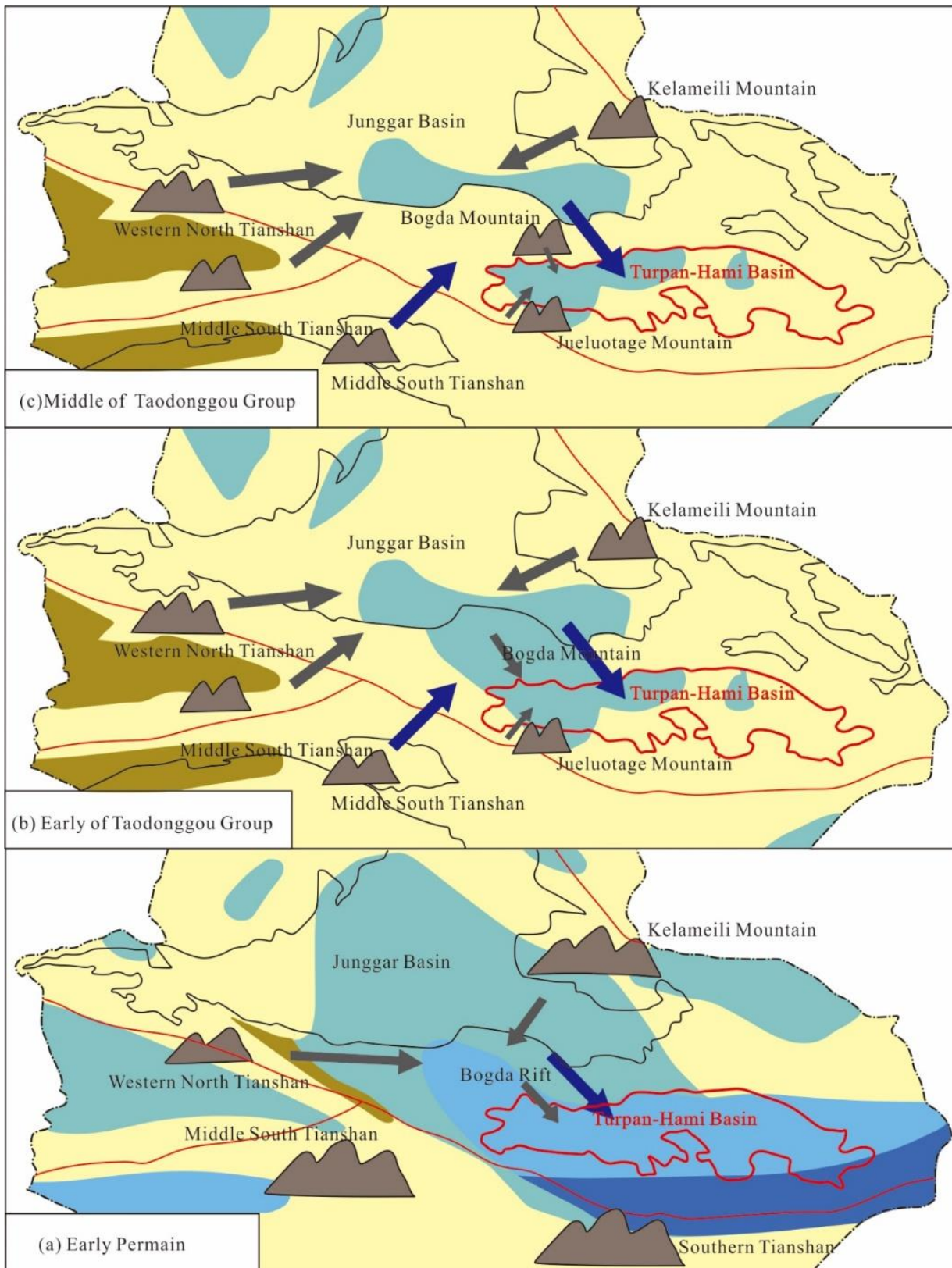
745 **Figure 11: Tectonic setting of source area in Taodonggou Group mudstone: (a) La-Th-Sc ternary diagram (modified after Zhu et al., 2021);**  
 746 **(b) Th-Co-Zr/10 ternary diagram (modified after Zhu et al., 2021); (c) cross plot of  $Al_2O_3/SiO_2$  and  $Fe_2O_3+MgO$  (modified after Bhatia,**  
 747 **1983); (d) cross plot of  $TiO_2$  and  $Fe_2O_3+MgO$  (modified after Bhatia, 1983); (e) cross plot of  $SiO_2$  and  $Al_2O_3/SiO_2$  (modified after Roser**  
 748 **and Korsch, 1988)**



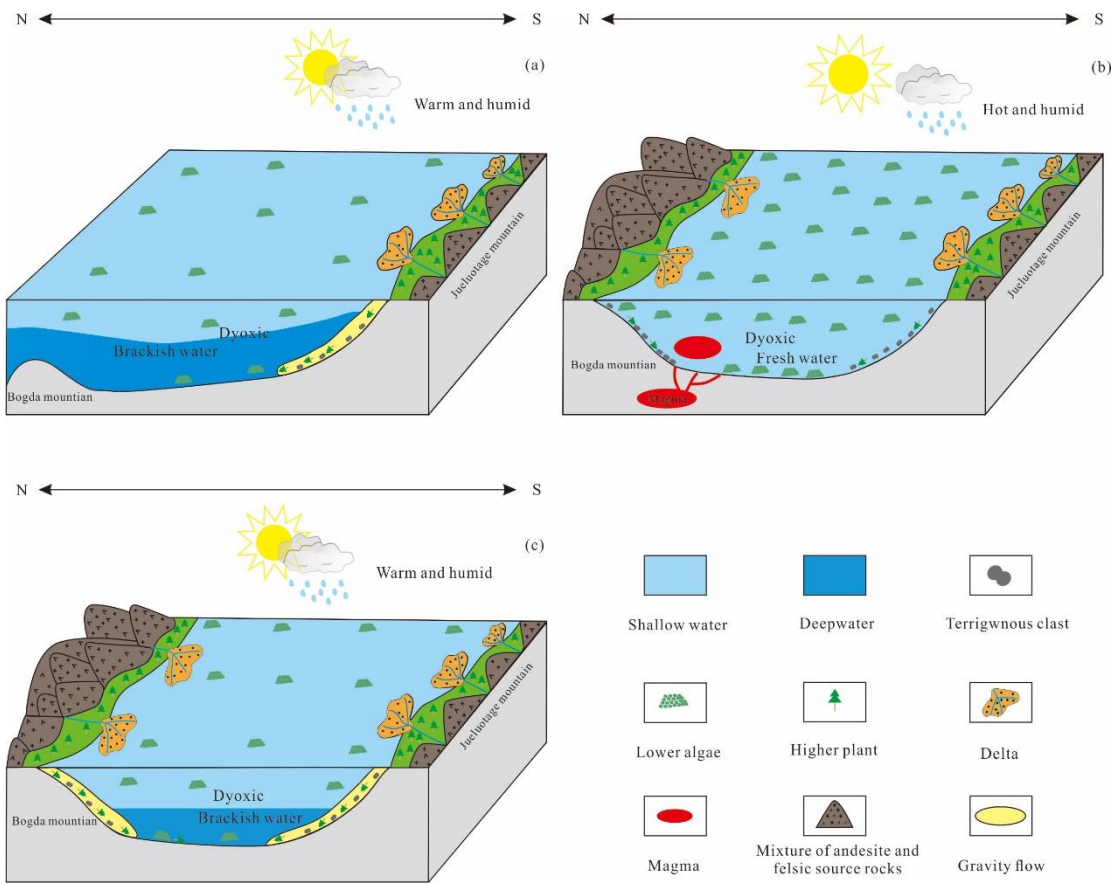
749  
 750 **Figure 12: The geochemical profile of the Taodonggou Group in YT1 well**



751  
 752 **Figure 13: Parent rock type of Taodonggou Group in YT1 well (Data of Lucaogou Formation in Junggar Basin are from Li et al., 2020):**  
 753 **(a) Th/Sc and Zr/Sc intersection diagram(modified after Floyd and Leveridge, 1987); (b) La/Th and Hf intersection diagram(modified**  
 754 **after Floyd and Leveridge, 1987); (c) Co/Th and La/Sc intersection diagram(modified after Wronkiewicz and Condie, 1987); (d)  $TiO_2$  and**  
 755 **Zr intersection diagram; (e) La/Yb and  $\Sigma REE$  intersection diagram (modified after Allègre and Minster, 1978)**



756  
757 **Figure 14: Provenance location from Early Permian to Middle Permian in Tianshan area (modified after Zhao et al., 2020): (a) Early**  
758 **Permian; (b) Early of Taodonggou Group; (c) Middle to later of Taodonggou Group**



759

760

**Figure 15: Middle Permian source sink system and lake basin evolution history of Turpan-Hami basin: (a) Early Taodonggou Group; (b)**

761

**Middle Taodonggou Group; (c) Late Taodonggou Group**

Table.1 Mineral composition of Taodonggou Group mudstone in YT1 well

Samples	Depth/m	Minerals content/%							
		Quartz	K-fledspar	Plagioclase	Calcite	Siderite	Pyrite	Barite	Clay
YT1-1	6084	29.4	0.7	1.8	23.7	/	/	13.3	31.1
YT1-2	6092	30.1	1.1	5.4	26.9	/	/	2.1	34.4
YT1-3	6102	41.9	/	2.5	18.1	/	/	3.2	34.3
YT1-4	6113	35.7	0.5	2.9	10.8	/	/	2.8	47.3
YT1-5	6122	40.5	0.1	2.7	19.4	/	/	4.6	32.7
YT1-6	6129	39.2	0.6	2.1	19.7	/	/	4	34.4
YT1-7	6136	27.9	0.3	0.8	42.8	/	/	4.3	23.9
YT1-8	6140	31.2	0.6	0.6	22.1	/	/	5.6	39.9
YT1-9	6143	34	0.4	0.2	14	/	/	4.5	46.9
YT1-10	6144.7	33.6	2.1	3.7	11.4	2.1	2.8	3.5	40.8
YT1-11	6145.3	37	/	3.7	10.6	1.4	/	2.1	45.2
YT1-12	6145.8	38.4	1.7	2.2	12.5	/	/	3.1	42.1
YT1-13	6147	37.9	/	/	1	/	1.4	1.2	58.5
YT1-14	6151	59.2	0.5	0.2	1.3	/	2.1	/	36.7
YT1-15	6154	21.8	0.8	0.8	1.8	/	/	3.9	70.9
YT1-16	6161	17.2	2.3	4.8	35.4	2	/	5	33.3

Table. 2 Major elements of Taodonggou Group mudstone in well YT1

Samples	Depth/m	Content/%										CIA	P/Ti	K <sub>2</sub> O/Al <sub>2</sub> O <sub>3</sub>
		SiO <sub>2</sub>	CaO	Al <sub>2</sub> O <sub>3</sub>	Fe <sub>2</sub> O <sub>3</sub>	K <sub>2</sub> O	TiO <sub>2</sub>	Na <sub>2</sub> O	MgO	P <sub>2</sub> O <sub>5</sub>	MnO			
YT1-1	6084	43.79	19.05	11.65	5.32	3	1.35	1.15	1.1	0.9	0.3	68.71	0.49	0.26
YT1-2	6092	54.32	14.01	14.96	6.74	3.39	1.37	1.5	1.34	0.29	0.15	70.1	0.15	0.23
YT1-3	6102	56.63	14.36	11.66	5.42	3.38	1.24	1.23	1.36	0.16	0.19	66.63	0.09	0.29
YT1-4	6113	56.92	7.38	17.52	7.93	4.2	1.28	1.22	1.55	0.21	0.14	72.55	0.12	0.24
YT1-5	6122	51.15	12.62	15.25	7.55	3	1.33	1.2	1.15	0.3	0.34	73.85	0.17	0.20
YT1-6	6129	62.28	4.49	16.07	5.93	3.5	1.15	1.68	0.8	1.17	0.12	70.08	0.74	0.22
YT1-7	6136	52.44	9.31	16.57	8.63	2.54	1.5	1.55	0.66	0.37	0.34	74.57	0.18	0.15
YT1-8	6140	55.37	3.01	21.11	9.64	2.63	1.42	1.5	0.49	0.15	0.24	78.92	0.08	0.12
YT1-9	6143	60.24	2.76	21.27	8.73	1.92	1.76	0.84	0.36	0.23	0.22	85.5	0.09	0.09
YT1-10	6144.7	61.08	2.75	24.16	7.54	0.99	1.82	0.3	0.36	0.21	0.06	93.83	0.08	0.04
YT1-11	6145.3	61.02	2.94	25.39	6.84	0.59	1.84	0.31	0.36	0.26	0.06	95.45	0.10	0.02
YT1-12	6145.8	60.32	5.41	21.32	7.29	0.72	1.85	0.34	0.32	0.21	0.06	93.84	0.08	0.03
YT1-13	6147	60.76	1.83	25.75	7.68	0.68	1.95	0.19	0.35	0.25	0.05	96.07	0.09	0.03
YT1-14	6151	70.11	2.44	12.83	7.28	0.97	1.31	0.34	0.27	0.15	0.05	88.59	0.09	0.08
YT1-15	6154	49.39	1.92	25.41	12.25	2.84	2.87	1.57	0.46	0.15	0.06	80.97	0.04	0.11
YT1-16	6161	43.11	9.56	18.04	14.17	2.83	4.22	1.9	0.77	1.03	0.25	73.12	0.18	0.16



Table.3 Characteristics of Trace elements in Taodonggou Group mudstone

Samples	YT1-1	YT1-2	YT1-3	YT1-4	YT1-5	YT1-6	YT1-7	YT1-8	YT1-9	YT1-10	YT1-11	YT1-12	YT1-13	YT1-14	YT1-15	YT1-16
Depth/m	6084	6092	6102	6113	6122	6129	6136	6140	6143	6144.7	6145.3	6145.8	6147	6151	6154	6161
Be	0.952	1.12	1.67	1	1.52	1.26	1.74	2.17	1.79	1.31	1.35	1.42	0.711	1.77	2.05	1.55
Sc	9.02	11.9	15.5	11.7	13.6	13.1	15.6	16.2	21.2	11.4	13.2	12.3	7	24	26	17.6
V	87.3	64.2	72	59.5	106	89.2	100	88.5	88.7	122.3	114.6	131.6	177	145	124	199
Cr	27.4	21.2	31.8	27.3	40.1	43	40.1	45.1	54.8	48.5	47.6	44.5	43	63	51	40.2
Co	9.46	12.4	14.9	13.3	11.9	12.6	13.7	18.2	27.6	22.3	21.7	20.6	18.7	24.8	36.9	30.4
Ni	25.5	27.8	36.7	32.5	32.6	33.2	37.8	37.2	47.5	36.8	35.7	34.6	27.3	41.7	55.4	17.9
Cu	34.2	33.1	44.8	34.6	51.2	41.8	39.9	50.8	48.9	52.6	50.3	51.4	57.3	55.8	64.4	71.2
Zn	125	79	92.4	96.1	69.8	90.4	74.4	67.9	78.7	64.6	63.2	65.8	44.1	70.4	114	218
Ga	17.81	20.1	23.3	19	24.8	21.9	15.1	13.2	16.1	14.5	12.7	13.7	7.14	12.7	19.2	17.3
Rb	54.5	64.6	73.5	50.4	60	33.5	33.9	16	17.9	15.6	14.6	14.6	13.6	14.2	21	20.7
Sr	758	357	420	422	291	414	269	151	199	214	244	224	63.9	126	263	393
Mo	1.29	0.661	0.866	1.24	1.09	1.44	1.17	1.23	2.68	3.02	2.88	3.14	3.86	2.14	1.18	1.28
Ba	483.83	735.7	633	547.28	159.24	547.66	326.49	465.2	565	503	516	505	427	254	303.56	424.35
B	46.31	71.3	81.4	67.4	64.5	55.4	60.2	41.3	49.6	44.6	52.6	41.4	41.5	39.7	56.2	54.1
Th	9.16	6.03	7.31	6.43	8.38	12.4	10.3	10.4	10	9.12	8.33	8.86	6.17	7.32	9.96	3.13
U	2.13	1.8	1.83	2.14	1.66	3.1	3.17	2.43	2.06	3.1	3.06	2.89	3.2	2.66	2.42	0.73
Zr	82.7	99.3	124	97.1	107	112	123	132	162	128.8	130.2	123.6	70.8	130.4	192	215
Hf	2.6	3.77	4.29	3.51	3.87	4.03	4.45	4.76	5.52	4.76	3.94	4.01	2.23	3.21	6.13	6.29
Sr/Ba	1.57	0.49	0.66	0.77	1.83	0.76	0.82	0.32	0.35	0.43	0.47	0.44	0.15	0.5	0.87	0.93
Ga/Rb	0.33	0.31	0.32	0.38	0.41	0.65	0.45	0.83	0.9	0.93	0.87	0.94	0.53	0.89	0.91	0.84
B/Ga	2.6	3.55	3.49	3.55	2.6	2.53	3.99	3.13	3.08	3.08	4.14	3.02	5.81	3.13	2.93	3.13
Rb/K/(10 <sup>-4</sup> )	21.87	22.94	26.18	14.45	24.08	11.52	16.07	7.32	11.22	18.97	29.79	24.41	24.08	17.63	8.9	8.81
V/Cr	3.19	3.03	2.26	2.18	2.64	2.07	2.49	1.96	1.62	2.52	2.41	2.96	4.12	2.3	2.43	4.95
V/(V+Ni)	0.77	0.7	0.66	0.65	0.76	0.73	0.73	0.7	0.65	0.77	0.76	0.79	0.87	0.78	0.69	0.92
$\bar{C}$	0.22	0.32	0.26	0.54	0.43	0.53	0.61	1.19	1.38	1.61	1.56	1.03	2.42	1.64	1.56	0.93

Table 4 Enrichment Factors of the Taodonggou Group mudstone after AS transformation

Samples	$X_{EF}$																	
	Be	Sc	V	Cr	Co	Ni	Cu	Zn	Ga	Rb	Sr	Mo	Ba	B	Th	U	Zr	Hf
YT1-1	0.43	0.11	0.92	0.42	0.68	0.51	1.04	1.80	1.28	0.53	3.66	0.63	1.14	0.68	1.05	0.78	0.71	1.28
YT1-2	0.39	0.12	0.53	0.25	0.70	0.44	0.78	0.89	1.13	0.49	1.34	0.25	1.35	0.82	0.54	0.52	0.66	1.44
YT1-3	0.75	0.19	0.76	0.48	1.07	0.74	1.36	1.33	1.68	0.72	2.03	0.43	1.49	1.20	0.83	0.67	1.06	2.11
YT1-4	0.30	0.10	0.42	0.28	0.64	0.43	0.70	0.92	0.91	0.33	1.36	0.41	0.86	0.66	0.49	0.52	0.55	1.15
YT1-5	0.52	0.13	0.85	0.47	0.66	0.50	1.19	0.77	1.37	0.45	1.07	0.41	0.29	0.73	0.73	0.47	0.70	1.45
YT1-6	0.41	0.12	0.68	0.47	0.66	0.48	0.92	0.94	1.14	0.24	1.45	0.51	0.94	0.59	1.03	0.83	0.69	1.44
YT1-7	0.55	0.14	0.74	0.43	0.69	0.53	0.85	0.75	0.77	0.23	0.91	0.40	0.54	0.62	0.83	0.82	0.74	1.54
YT1-8	0.54	0.11	0.51	0.38	0.72	0.41	0.85	0.54	0.52	0.09	0.40	0.33	0.61	0.34	0.66	0.49	0.62	1.29
YT1-9	0.44	0.14	0.51	0.46	1.09	0.52	0.81	0.62	0.64	0.10	0.53	0.72	0.73	0.40	0.63	0.42	0.76	1.49
YT1-10	0.28	0.07	0.62	0.36	0.77	0.36	0.77	0.45	0.50	0.07	0.50	0.72	0.57	0.32	0.50	0.55	0.53	1.13
YT1-11	0.28	0.08	0.55	0.33	0.72	0.33	0.70	0.42	0.42	0.07	0.54	0.65	0.56	0.36	0.44	0.52	0.51	0.89
YT1-12	0.35	0.08	0.76	0.37	0.81	0.38	0.85	0.52	0.54	0.08	0.59	0.84	0.65	0.33	0.55	0.58	0.58	1.08
YT1-13	0.14	0.04	0.84	0.30	0.61	0.25	0.79	0.29	0.23	0.06	0.14	0.86	0.46	0.28	0.32	0.53	0.27	0.50
YT1-14	0.72	0.27	1.39	0.87	1.62	0.76	1.54	0.92	0.83	0.13	0.55	0.95	0.54	0.53	0.76	0.89	1.01	1.43
YT1-15	0.42	0.15	0.60	0.36	1.22	0.51	0.90	0.75	0.63	0.09	0.58	0.27	0.33	0.38	0.52	0.41	0.75	1.38
YT1-16	0.45	0.14	1.35	0.39	1.41	0.23	1.40	2.03	0.81	0.13	1.23	0.41	0.65	0.51	0.23	0.17	1.19	2.00
Average	0.41	0.12	0.73	0.40	0.87	0.44	0.93	0.79	0.75	0.20	0.91	0.56	0.68	0.50	0.59	0.55	0.68	1.29

Table 5 Characteristics of REE in Taodonggou Group mudstone

Samples	Depth/m	Content/ppm															$\Sigma$ REE	LREE	MREE	HREE	(La/Yb) <sub>N</sub>
		La	Ce	Pr	Nd	Sm	Eu	Gd	Tb	Dy	Ho	Er	Tm	Yb	Lu						
YT1-1	6084	31.70	57.70	6.73	28.80	5.14	1.46	5.19	0.72	3.89	0.68	2.17	0.30	2.12	0.352	146.953	124.930	17.077	4.946	10.081	
YT1-2	6092	27.30	47.80	5.51	22.90	4.79	0.84	4.13	0.73	4.25	0.71	2.40	0.37	2.56	0.408	124.695	103.510	15.447	5.738	7.190	
YT1-3	6102	27.30	48.30	5.62	23.10	4.71	1.32	4.17	0.80	4.63	0.88	2.68	0.41	2.89	0.464	127.271	104.320	16.511	6.440	6.369	
YT1-4	6113	26.40	45.60	5.20	22.20	4.37	0.96	4.09	0.68	3.88	0.72	2.35	0.36	2.56	0.408	119.783	99.400	14.705	5.678	6.953	
YT1-5	6122	32.60	62.80	7.61	31.70	6.56	1.96	5.77	0.98	5.35	0.97	2.89	0.43	2.92	0.429	162.971	134.710	21.590	6.671	7.527	
YT1-6	6129	33.10	80.10	7.48	31.70	6.19	0.62	5.98	0.99	5.58	0.99	3.01	0.50	3.31	0.564	180.108	152.380	20.345	7.383	6.742	
YT1-7	6136	33.50	66.40	7.70	31.20	6.19	1.18	5.46	0.91	5.24	0.96	3.05	0.49	3.18	0.454	165.914	138.800	19.936	7.178	7.102	
YT1-8	6140	35.90	65.80	7.23	29.20	5.47	1.65	4.96	0.96	5.35	0.96	2.97	0.47	3.01	0.426	164.346	138.130	19.344	6.872	8.041	
YT1-9	6143	39.00	73.40	9.60	40.00	7.18	1.44	5.64	1.02	5.91	1.08	3.45	0.52	3.41	0.519	192.169	162.000	22.270	7.899	7.711	
YT1-10	6144.7	32.60	66.43	7.34	26.40	6.31	0.98	4.82	0.84	4.97	0.86	3.12	0.33	3.21	0.436	158.646	132.770	18.130	7.096	6.847	
YT1-11	6145.3	27.90	62.23	5.23	23.20	5.42	1.04	4.46	0.92	5.41	0.88	2.88	0.44	3.02	0.423	143.453	118.560	17.880	6.763	6.228	
YT1-12	6145.8	30.20	65.60	5.64	25.40	5.93	1.02	5.01	0.47	4.54	0.91	2.94	0.46	3.01	0.501	151.631	126.840	5.531	6.911	6.764	
YT1-13	6147	8.84	16.80	1.75	6.90	1.39	0.30	1.32	0.27	1.87	0.39	1.27	0.22	1.67	0.265	43.247	34.290	5.531	3.426	3.569	
YT1-14	6151	39.40	73.60	8.64	33.60	4.22	1.84	4.32	1.21	5.83	1.03	3.42	0.43	2.98	0.392	180.912	155.240	5.531	7.222	8.914	
YT1-15	6154	52.60	105.00	12.30	50.80	9.09	2.45	7.65	1.25	7.14	1.16	3.86	0.57	3.62	0.510	257.997	220.700	28.740	8.557	9.796	
YT1-16	6161	39.70	85.70	11.10	52.10	9.76	2.29	8.33	1.34	7.47	1.25	3.75	0.52	3.39	0.502	227.206	188.600	30.440	8.166	7.895	

LREE = La + Ce + Pr + Nd; MREE = Sm + Eu + Gd + Tb + Dy + Ho; HREE = Er + Tm + Yb + Lu; (La/Yb)<sub>N</sub> = (La/Yb)/(La/Yb)<sub>chondrite</sub>